Response to Reviewer #3

‘Spatial variability of snow precipitation and accumulation in COSMO-WRF simulation and radar estimations over complex terrain’

F. Gerber (gerberf@slf.ch), N. Besic, V. Sharma, R. Mott, M. Daniels, M. Gabella, A. Berne, U. Germann, M. Lehning

Dear Sir or Madam,
We are thankful for your positive comments and for the feedback, which helped us to improve the manuscript. Reviewer comments are printed in black. Our answers and comments are printed in blue. Main changes done in the manuscript are printed in italic. **All pages and line numbers refer to the track-changes version of the manuscript (attached below).**

General comment:

The English should also be improved before publication of the manuscript.

We tried to improve the English and readability of the manuscript.

These are the specific comments:

1. The organization of the introduction should be improved. The goal of the study is not clearly stated. There is a question at the end of p.2. The following paragraph continues with the literature review and then, they elaborate a little more on the objective of the study. I would suggest focusing first on the literature review, listing the gaps in the field of snow redistribution near the surface, the objective of the study and how it will be addressed.

We rearranged the introduction such that it hopefully is more reader-friendly. We tried to give it a better structure and clearly highlight the research questions. At the end of the introduction we added an extended paragraph explaining the structure of the paper and related objectives (P. 2-4).

2. P. 4, line 1, do you mean northerly? The sub-domain is located on south-easterly of the domain.

Here, we only refer to the location of domains d01 and d02. We indeed mean that we shifted domain d02 toward the eastern boundary of domain d01, which is visible in the left panel of Figure 1 (d01: dark red, d02: red).

3. P. 4, line 5, should probably give the precise dates here.

We added the exact dates of the event and additionally refer to Section 2.5, where we also give information about the different snowfall event.

P. 5, l. 15-17: “*Simulations are performed for three snow precipitation events on 31 January 2016, 4 February 2016 and 5 March 2016 (Sect. 2.5).”*

4. P. 5, line 10, the units should not be in italic. Please modify here and everywhere in the manuscript.

Done.

5. P.7, line 4: Should it be at noon instead of “during”? I am not sure what the authors mean here.

We agree that “during noon” has to be changed. We change it to *“around midday”* to make sure we are talking about few hours around midday (P. 8, l. 31).

6. P.10, Figure 2: The font on the figures is too small. Letters should be added to all panels to help following the text.

We increased the font sizes in Figure 2 and added letters for each panel. Cross references in the text are adapted accordingly.

7. P.11, Figure 3: The font is too small. It is very hard to read.

As for Figure 2 (see above).

8. P. 11, line 8 and 9: Please clarify the sentence: “The introduction of drops in relative humidity by WRF may be due to an overestimation of subsidence in the model.” Subsidence is not necessarily directly linked to relative humidity. It contributes to warm the air adiabatically, which leads to drier conditions.

We try to clarify by (P. 14, l.3-6): "*Thus, the introduction of a higher variability in relative humidity in our WRF simulations may be due to strong subsidence and lifting, which lead to an overestimation of adiabatic cooling or warming and hence to an overestimation of humidity generation and decay. Additionally, differences between modeled and measured relative humidity may be due to measurement uncertainties.”*

9. P.12, line 12: Similar comment as #7.

The authors are not sure what you are referring to. Comment #7 is about Figure 2 but there is no figure on P.12, line 12. Anyway the paragraph about wind speeds (which contains line 12 on P. 12) has been rewritten given reviewer comments in reviews #1 and #2.

10. P.13, line 12: What do you mean by “advection in the microphysics scheme”? The microphysics scheme predicts the mixing ratio and the number concentration of hydrometeor through phase changes, collection and fall speed. I think that advection of hydrometeor is computed in WRF. Please clarify this sentence.

The microphysics scheme by Morrison et al., 2005 “…contains kinetic equations for the mixing ratio q, and number concentration, N, …”. The spatial derivatives of mixing ratio and number concentration contain an advection term (first term on the right hand side (rhs) in eqs. (1) and (2)), a sedimentation term which depends on the terminal fall velocity ($V_{qx,}$ second term on the rhs in eqs. (1) and (2)) and a turbulent diffusion term (third term on the rhs in eqs. (1) and (2)). All the other terms on the rhs in eqs. (1) and (2) are source and sink terms due to microphysical processes. For more details, please, consult Morrison et al., 2005.

$$\frac{\partial q}{\partial t} = -\nabla \cdot (\mathbf{v}q) + \frac{\partial}{\partial z}(V_{qx}) + \nabla_D q + \left(\frac{\partial q}{\partial t}\right)_{\text{PRO}} + \left(\frac{\partial q}{\partial t}\right)_{\text{COND/DEP}} + \left(\frac{\partial q}{\partial t}\right)_{\text{AUTO}} + \left(\frac{\partial q}{\partial t}\right)_{\text{COAG}} + \left(\frac{\partial q}{\partial t}\right)_{\text{MLT/FRZ}} + \left(\frac{\partial q}{\partial t}\right)_{\text{MULT}}, \quad (1)$$

$$\frac{\partial N}{\partial t} = -\nabla \cdot (\mathbf{v}N) + \frac{\partial}{\partial z}(V_{Nx}) + \nabla_D N + \left(\frac{\partial N}{\partial t}\right)_{\text{PRO}} + \left(\frac{\partial N}{\partial t}\right)_{\text{EVAP/SUB}} + \left(\frac{\partial N}{\partial t}\right)_{\text{AUTO}} + \left(\frac{\partial N}{\partial t}\right)_{\text{SELF}} + \left(\frac{\partial N}{\partial t}\right)_{\text{COAG}} + \left(\frac{\partial N}{\partial t}\right)_{\text{MLT/FRZ}} + \left(\frac{\partial N}{\partial t}\right)_{\text{MULT}}, \quad (2)$$

11. P.14, Figure 4: The font is too small. It is very hard to read. It is also hard to compare among each other because the scale is different. Please use the same scale, if possible.

To make it more intuitive to compare the patterns, we decided to show the deviation from mean precipitation, which we can show with the same colorbars. We hope this improves the readability of the figure. Additionally, we increased the font size. Using the same colorbar for all panels showing precipitation distributions was not possible due to strongly differing precipitation distributions.

12. P.15, Figure 5: The lines associated with the figure axis are missing on the figure. The x-axis could be called the Data sources (or something like that). I think that the dates could be at the top of each panel. Also please add letters to panels for clarity.

This figure only contains one panel, thus we think that is not necessary to add panel labels. The x-axis in this figure represents time. Grouped box plots for each date are shown. The data sources are given in the legend and thus we think it is not necessary to state this more specifically. We agree that the horizontal lines associated with precipitation rates given on the y-axis were not well visible. We increase the line thickness of these lines and chose a darker color to hopefully make this figure more reader-friendly.

13. P.16, line 3: The following sentence states that the model is overestimating precipitation: "… model tends to overestimate precipitation for higher resolution…". As mentioned in line 21, there is also uncertainty in the radar derived precipitation amounts. It would be good to add 1-2 sentences about his issue. For example, did you try other S-R relationship to derive precipitation information from the radar?

Indeed, a fair point! We have not compared different S-Z relationships, but rather adopted the commonly used Finish formula. Although the uncertainty in the Z-S parameters may lead to significant uncertainty in the total amount, it should not strongly affect the spatial variability (quantified by the normalized variogram or autocorrelation). To be rigorous, we nevertheless follow the suggestion of the reviewer and explicitly mention the possible uncertainty associated with radar estimates.

P. 18, l. 22-25: "*Although radar estimates are based on a referent S-Z relationship, the employed formula (Eq. 1) is not immune to the potential estimation errors. Therefore, despite reasonably assuming that the potential estimation errors should not significantly influence the variability and the intensity of the precipitation fields, while drawing conclusions we have subjectively considered the impact of imperfections characterizing such an empirical formula.*"

Reference:

Morrison, H., Curry, J. A., and Khvorostyanov, V. I.: A New Double-Moment Microphysics Parameterization for application in Cloud and Climate Models. Part I: Description, Journal of Atmospheric Sciences, 62, 1665 – 1677, https://doi.org/10.1175/JAS3446.1, 2005.

Spatial variability of snow precipitation and accumulation in COSMO–WRF simulations and radar estimations over complex terrain

Franziska Gerber[1,2], Nikola Besic[3,4], Varun Sharma[1], Rebecca Mott[2,5], Megan Daniels[6], Marco Gabella[4], Alexis Berne[3], Urs Germann[4], and Michael Lehning[1,2]

[1]Laboratory of Cryospheric Sciences, School of Architecture and Civil Engineering, École Polytechnique Fédérale de Lausanne, Lausanne, Switzerland.
[2]WSL Institute for Snow and Avalanche Research SLF, Davos, Switzerland.
[3]Environmental Remote Sensing Laboratory, School of Architecture and Civil Engineering, École Polytechnique Fédérale de Lausanne, Lausanne, Switzerland.
[4]Radar, Satellite, Nowcasting Departement, MeteoSwiss, Locarno, Switzerland.
[5]Institute of Meteorology and Climate Research, Atmospheric Environmental Research (KIT/IMK-IFU), KIT-Campus Alpin, Garmisch-Partenkirchen, Germany.
[6]unaffiliated, Sydney, Australia.

Correspondence to: F. Gerber (gerberf@slf.ch)

Abstract. Snow distribution in complex alpine terrain and its evolution in the future climate is important in a variety of applications including hydro-power, avalanche forecasting and fresh water resources. ~~However, the relative importance of processes such as cloud-dynamics and pure particle-flow interactions is still barely known and models are essential to investigate these processes~~ However, it is still challenging to quantitatively forecast precipitation especially over complex terrain, where the interaction between local wind and precipitation fields strongly affects snow distribution at the mountain ridge scale. Therefore, it is essential to retrieve high-resolution information about precipitation processes over complex terrain. Here, we present very high resolution Weather Research and Forecasting model (WRF) simulations (COSMO–WRF), which are initialized by 2.2 km resolution Consortium for Small-scale Modeling (COSMO) ~~reanalysis (COSMO–WRF)~~analysis. To assess the ability of COSMO–WRF to represent spatial snow precipitation patterns, they are validated against operational weather radar measurements. Estimated ~~WRF~~ COSMO–WRF precipitation is generally higher than estimated radar precipitation, most likely due to an overestimation of orographic precipitation enhancement in the model. The high precipitation ~~also leads~~ amounts also lead to a higher spatial variability in the model ~~at the scale of 10 km~~compared to radar estimates. Overall, an autocorrelation and scale analysis of radar and ~~WRF precipitation patterns show that WRF captures the variability relative to the domain-wide~~ COSMO–WRF precipitation patterns at a horizontal grid spacing of 450 m show that COSMO–WRF captures the spatial variability normalized by the domain-wide variability of precipitation patterns down to the scale of few kilometers~~, but misses quite substantial~~. However, simulated precipitation patterns systematically show a lower variability on the smallest scales of a few 100 ~~meters. However~~m compared to radar estimates. A comparison of spatial variability for different model resolutions gives evidence for an improved representation of local precipitation processes at a horizontal resolution of 50 m compared to

450 m. Additionally, differences of precipitation between 2830 m above sea level and the ground indicate that near-surface processes are active in the model.

1 Introduction

In many regions of the world, e.g. the Alps or the Californian Sierra Nevada, snow is the main source of fresh water. Additionally, it is an important resource for hydro-power and is ~~essential~~ crucial for winter tourism in skiing areas (Schmucki et al., 2017). Thus, especially in a changing climate, it is essential to improve the understanding of processes forming the seasonal snow cover. Improving the ability of weather forecast models to represent the spatial variability of snowfall is further crucial to efficiently manage fresh water and hydro-power. Moreover, as snow is a potential danger in terms of avalanches, improved knowledge about the distribution of snow is crucial for avalanche forecasting and prevention.

Snow accumulation patterns at a mountain-range scale are known to be strongly dependent on blocking and lifting processes including large-scale orographic precipitation enhancement (e.g. Houze, 2012; Stoelinga et al., 2013), which is related to the large-scale atmospheric circulation. However, for a long time little knowledge was available about the spatial distribution of snow on a mountain-slope or river-catchment scale. Only in recent years improvements in technology allowed the investigation of mountain-slope scale snow distribution ~~(e.g. Grünewald et al., 2010; Prokop, 2008; Deems et al., 2006)~~(e.g. Deems et al., 2006; Prokop, Terrestrial and airborne laser scanning reveal annually persistent patterns of peak-of-winter snow accumulation distribution on river-catchment scales (Schirmer et al., 2011; Scipión et al., 2013), which is found to be consistent with few dominant snowfall events of the season. Reported scale breaks in fractal analysis of snow accumulation patterns are mainly at scales < 100 m and represent the occurrence of a change in dominant processes (e.g. Deems et al., 2008). On very small-scales snow accumulation patterns are assigned to wind redistribution of snow (e.g. Mott et al., 2011; Vionnet et al., 2017). Vegetation effects were found to be dominant at small scales and terrain effects dominate on scales up to 1 km (Deems et al., 2006; Trujillo et al., 2012; Tedesche et al., 20 Different dominant scales are reported for different slope expositions relative to the wind direction (Schirmer and Lehning, 2011). Furthermore, Schirmer et al. (2011) could show that snow accumulation smooths the underlying terrain, reducing the small-scale spatial variability of topography. While most studies addressed variability of snow accumulation, the combined scale analysis of snow accumulation and snow precipitation patterns by Scipión et al. (2013) reveals much smoother patterns in snow precipitation at about 300–600 m above ground compared to final snow accumulation at the ground on scales up to 2 km This stresses the importance of pre-depositional near-surface and post-depositional processes for snow accumulation patterns.

Driving processes of snow accumulation on ~~a~~ the mountain-ridge scale were addressed in numerous studies, which reveal two main pre-depositional processes. On the one hand, mountain-ridge scale precipitation and accumulation are influenced by local ~~cloud-dynamic~~ cloud-dynamical processes (Choularton and Perry, 1986; Dore et al., 1992; Zängl, 2008; Zängl et al., 2008; Mott et al., 2014). On the other hand, ~~pure~~ particle-flow interactions (i.e. the influence of the local flow field on the pathways of snow particles and particle distribution in the air) determine snow accumulation patterns in mountainous terrain (Colle, 2004; Zängl, 2008; Lehning et al., 2008; Dadic et al., 2010; Mott et al., 2010, 2014). On ~~a~~ the mountain-ridge scale, Mott et al. (2014) ~~could document~~ documented the occurrence of a local event of orographic ~~enhancement of snowfall due to the occurrence~~ snowfall

enhancement. In their case study, the presence of a low-level cloud ~~acting as a feeder cloud, giving evidence for the local occurrence of small-scale orographic enhancement~~ gives evidence for precipitation enhancement favored by the seeder-feeder mechanism (e.g. Bergeron, 1965; Purdy et al., 2005). On similar scales, preferential deposition (Lehning et al., 2008) was found to cause enhanced snow accumulation on leeward slopes (e.g. Mott et al., 2010; Mott and Lehning, 2010). However, snow depth measurements in very steep terrain and corresponding local flow field measurements reveal even more complex particle-flow interactions (Gerber et al., 2017) than previously suggested ~~based on~~ by model studies. On even smaller scales the main driver of snow accumulation patterns is post-depositional snow transport by drifting and blowing snow, which is dependent on local topographic features and wind gusts ~~(Mott et al., 2010; Lehning and Fierz, 2008)~~(Lehning and Fierz, 2008; Mott et al., 2010).

Complex ~~topography-flow-precipitation interactions~~ terrain-flow-precipitation interactions (i.e. the effect of terrain-induced flow field variations on the precipitation formation and distribution), especially on ~~a~~ the mountain-ridge scale, still leave the relative importance of the different pre-depositional processes for snow accumulation and the frequency of occurrence barely known (Mott et al., 2014; Vionnet et al., 2017). Running a coupled simulation of the snowpack model Crocus and the atmospheric model Meso-NH in ~~large eddy~~ large-eddy simulation (LES) mode, Vionnet et al. (2017) ~~address~~ addressed the question of the relative importance of these different processes including snow redistribution by wind. Their results show that post-depositional snow transport dominates snow accumulation variability, but leaves the question of the relative importance of pre-depositional processes open.

~~To further investigate the relative importance~~ Given the small scale of these processes their relative importance may either be addressed based on very high resolution numerical simulations or based on spatially highly resolved precipitation measurements. Therefore, accurate model results and radar measurements ~~on~~ at high resolution are essential. ~~Here, we present a validation of very high resolution WRF simulations, which are forced by 2.2 km resolution Consortium for Small-scale Modeling (COSMO) reanalysis, with point measurements of temperature, relative humidity, wind speed and direction. Combining these WRF simulations with operational radar measurements we further present a variability analysis for snow precipitation on regional to mountain-ridge scale to address the question: How much snow precipitation variability is represented by~~ Both, however, are challenging to achieve and very high resolution ~~WRF simulations ?~~

simulations are still rare especially over complex terrain. Remote sensing techniques~~are the most, or perhaps the only, practical mean for obtaining relevant distributed measurements of the atmosphere~~, on the other hand, are the most important methods to obtain high-resolution spatial measurements of atmospheric properties at different atmospheric levels. They permit ~~us to obtain~~ to gain information about both the small- and the large-scale properties of the atmospheric processes. The particular place among these techniques belongs to the weather radar, due to its wide coverage, fine spatial resolution, and interaction of microwaves with the precipitation. These properties have been used ~~in inferring the orographic mechanisms~~to infer orographic precipitation enhancement, particularly in the case of liquid precipitation (Panziera et al., 2015). ~~In this contribution, we are~~

In this study, we present very high resolution WRF simulations, which are forced by 2.2 km resolution Consortium for Small-scale Modeling (COSMO) analysis and high resolution radar estimates making use of the recently renewed MeteoSwiss radar network (Germann et al., 2015) ~~,~~ and its adequate technical performances which allow observing precipitation in a ~~very~~ challenging, complex alpine environment. Combining the COSMO–WRF simulations with operational radar measurements,

we perform a variability analysis for snow precipitation at a regional to mountain-ridge scale to address the question: How much snow precipitation variability is represented by very high resolution WRF simulations?

~~In many studies the variability of small-scale snow accumulation has been addressed, reporting scale breaks in fractal analysis of snow accumulation patterns (e.g. Deems et al., 2008; Mott et al., 2011; Schirmer and Lehning, 2011). Reported scale breaks are mainly at scales <100 meters and represent the occurrence of a change in dominant processes (e.g. Deems et al., 2008). On very small-scales snow accumulation patterns are due to wind redistribution of snow (e.g. Vionnet et al., 2017).Vegetation effects were found to be dominant at smaller scales and terrain effects dominate on scales up to 1 km (Deems et al., 2006).Different dominant scales are reported for different slope expositions relative to the wind direction (Schirmer and Lehning, 2011).Furthermore, Schirmer et al. (2011) could show that snow accumulation smooths the underlying terrain, reducing the small-scale spatial variability of a certain slope.While most studies addressed variability of snow accumulation, the combined scale analysis of snow accumulation and snow precipitation patterns by Scipión et al. (2013) reveals much smoother patterns in snow precipitation at about 300–600 meters above ground compared to final snow accumulation at the ground on scales up to 2 km, stressing the importance of post-depositional processes for snow accumulation patterns.~~

Model simulations, radar measurements and analysis techniques are presented in Sect. 2. In a first part of the results and discussion (Sect. 3), we validate COSMO–WRF simulations against point measurements of temperature, relative humidity, wind speed and direction (Sect. 3.1). Spatial precipitation patterns in both, radar estimates and COSMO–WRF simulations, are presented in Sect. 3.2. Subsequently, we address the question how well the overall precipitation variability is represented in the model by analyzing the domain-wide statistics (Sects. 3.3). To address the spatial variability of precipitation patterns we present a discussion of dominant processes based on variograms and 2D-autocorrelation maps (Sect. 3.4). Variograms and autocorrelation analysis are widely used to address the spatial variability of snow accumulation and precipitation (e.g. Deems et al., 2008; M

While scale analysis has been performed multiple times for snow accumulation patterns on a local scale, we address measured and modeled snow precipitation patterns at the approximate elevation of the operational weather radar on Weissfluhgipfel at 2830 ~~meters~~ m above sea level (m asl) on a mountain-ridge to regional scale. Additionally, we analyze modeled ground precipitation without taking into account any post-depositional processes. Given the different scales of analysis compared to previous studies, here we address scales ~~on~~ at which local cloud dynamics and ~~pure~~ particle-flow interactions are expected to occur but leave out scales ~~on~~ at which snow accumulation is expected to be dominated by post-depositional snow redistribution. Following this analysis of spatial precipitation variability, which includes a discussion of dominant processes driving the spatial variability of precipitation patterns, Sect. 3.5 addresses the question if an increased model resolution may improve the representation of spatial variability in the model. Finally, our findings about the model performance, our analysis of the spatial variability of precipitation and future perspectives are wrapped up in a conclusion and outlook (Sect. 4).

2 Data and Methods

2.1 WRF model setup

Atmospheric simulations are performed with the non-hydrostatic and fully compressible Weather Research and Forecasting (WRF) model (Skamarock et al., 2008) version 3.7.1 for the region of Eastern Switzerland (~~Figure~~ Fig. 1). Simulations are set up with four one-way nested domains (d01–d04, ~~Figure~~ Fig. 1). Domain d01 has a horizontal resolution of 1350 ~~meters~~m, with 40 vertical levels and covers a region of a about 250 km times 320 ~~kilometers~~ km including eastern Switzerland and a portion of the neighboring countries (~~Figure~~ Fig. 1, Table 1, Supplementary Information S1). The three nests have horizontal resolutions of 450 ~~meters~~m, 150 ~~meters~~ m and 50 ~~meters~~ m using a nesting ratio (dx_{parent}/dx_{nest}) of 3. Domains d02–d04 have 40, 60 and 90 vertical levels, respectively, with the model top at 150 ~~mb~~ hPa using a preliminary version of vertical nesting (Daniels et al., 2016). Twenty and 40 vertical levels are refining the whole atmosphere in domains d03 and d04, respectively. Ten vertical levels in d04 are introduced to additionally refine the boundary layer. To make sure that there is plenty of domain for the model to adapt to the refined topography, domain d02 is shifted toward the eastern boundary of domain d01 as dominant wind directions are from a north-westerly and southerly direction. Domain d02 covers the ~~north-western part of Canton Grison (CH)~~central northern part of the Grisons, while domains d03 and d04 cover the surroundings of Davos and the upper Dischma valley, respectively (~~Figure~~ Fig. 1). ~~For domain d04 the boundary layer is setup with refined vertical levels.~~ Simulations are performed for three snow precipitation events ~~in January , February and March 2016.~~ on 31 January 2016, 4 February 2016 and 5 March 2016 (Sect. 2.5).

The parent domain is run with a planetary boundary layer (PBL) scheme (non-large eddy simulation (non-LES) mode), while the three nests are run in the ~~large eddy simulation mode(WRF-LES)~~LES mode. No strong differences were found when running domains d02 and d03 in ~~mesoscale~~ non-LES mode (not shown). Therefore and as we are interested in having an as good as possible representation of small-scale winds, we decided to run our simulations in the LES mode for all nested domains. ~~Additionally, this setup is consistent with previous~~ Domains d02 and d03 are within the 'gray zone' (Wyngaard, 2004). There are approaches omitting simulations in the 'gray zone' by the choice of a higher grid refinement ratio (Muñoz Esparza et al., 2017), which would be worth a sensitivity study. However, we use the well-tested 1:3 grid refinement ratio and keep our model setup consistent with the very high resolution simulations by Talbot et al. (2012), except that they perform separate simulations for the ~~mesoscale~~ non-LES and LES domains, while we run a nested simulation with one-way feedback for all four domains. ~~A combined simulation~~ Running a nested simulation of the non-LES and LES domains turned out to be necessary for precipitation to evolve properly in the LES domains, as hydrometeors cannot be used as a boundary condition for the parent domain but are fed to nested domains in WRF simulations. Subgrid scale turbulence is parametrized by the 1.5 order turbulent kinetic energy closure (Skamarock et al., 2008). For the ~~mesoscale~~ non-LES setup the Yonsei University PBL parameterization (YSU PBL, Hong et al., 2006) is used, which is considered to be one of the schemes showing the best performance over complex terrain (Gómez-Navarro et al., 2015). An adapted version of YSU PBL was shown to perform even better when taking into account subgrid-scale variability of the terrain (Jiménez and Dudhia, 2012; Gómez-Navarro et al., 2015). However, given our high model resolution we decided to keep the model simple and run the simulations with the

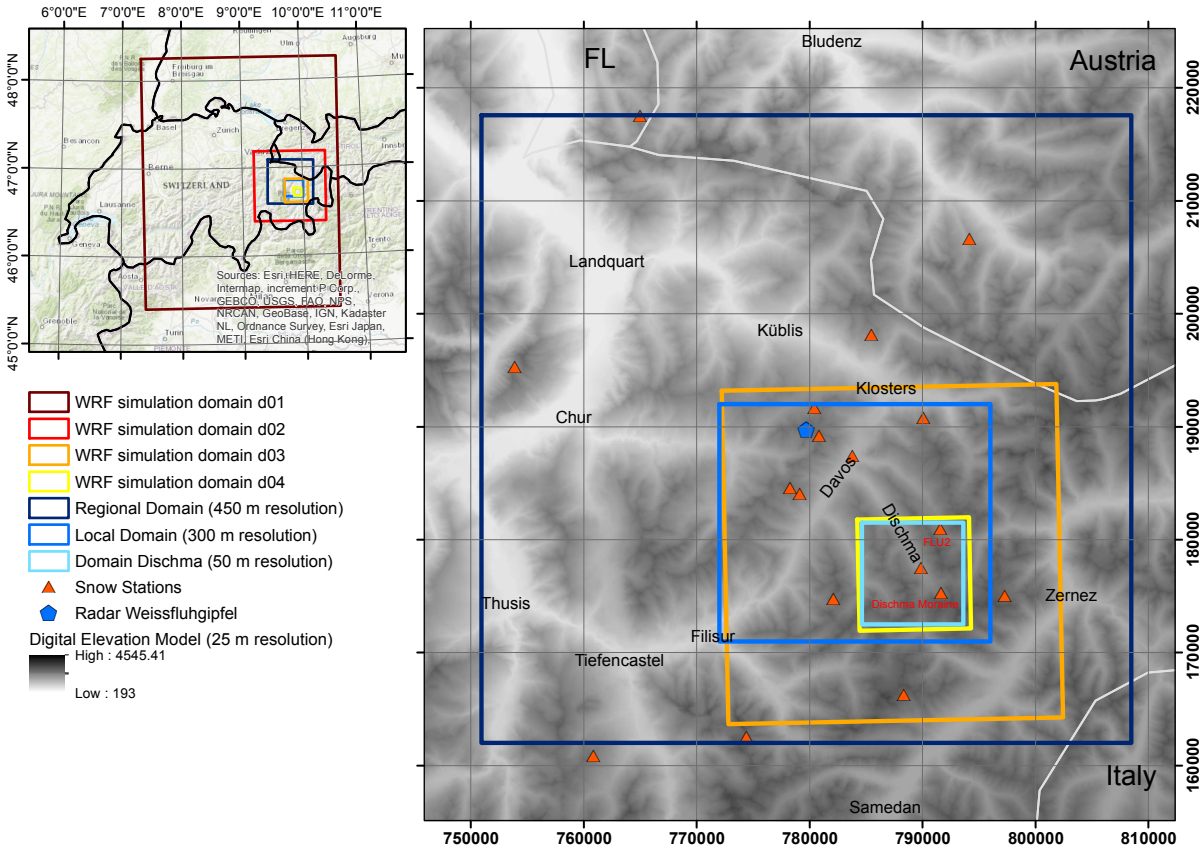

Figure 1. Overview over the study area in the eastern part of Switzerland surrounding Davos. WRF simulation domains (d01–d04, dark red to yellow) and evaluation domains (blue) give information on the simulation and evaluation setup. The 18 meteorological stations (red triangles) are within or very close to the regional domain. The two stations *Dischma Moraine* and *FLU2*, which are used to validate the model, are within domain Dischma. The operational weather radar is located on Weissfluhgipfel at approximately 2830 m above sea level (m asl, blue pentagon). Coordinates in the right panel are in Swiss coordinates CH1903LV03 (unit: ~~meters~~m). Shaded topography: dhm25 © 2018 swisstopo (5740 000 000).

standard YSU PBL. Landuse data is taken from the Corine dataset (European Environmental Agency, 2006) and translated to the USGS conventions ~~(Arnold et al., 2010; Pineda et al., 2004)~~(Pineda et al., 2004; Arnold et al., 2010). Soil type is set to *silty clay loam* for the whole domain. The link between the soil, which is modeled by the Noah ~~land surface~~ land-surface model with multi-parameterization options (Noah-MP, Niu et al., 2011; Yang et al., 2011), and the atmosphere is given by the MM5 Monin-Obukhov surface ~~model (Paulson, 1970; Dyer and Hicks, 1970; Webb, 1970; Beljaars, 1994; Zhang and Anthes, 1982)~~layer model (Paulson, 1970; Dyer and Hicks, 1970; Webb, 1970; Zhang and Anthes, 1982; Beljaars, 1994), which is based on the Monin-Obukhov similarity theory (Obukhov, 1971). For microphysics the Morrison 2-moment precipitation scheme (Morrison et al., 2005, 2009) is used, which was found to be one of the schemes, which most adequately simulate snow precipitation over

Table 1. Setup for the four nested domains (d01–d04) used in the WRF simulations. For the planetary boundary layer (PBL) the simulation mode is given, distinguishing between ~~mesoscale and large~~ non-large eddy simulation (LES) and LES settings. For ~~mesoscale setting~~ non-LES settings the PBL scheme is given. Additionally, the subgrid scale (SGS) turbulence parameterization is given for all four domains. *dx*, *dy* give the horizontal resolution. *Vertical levels* gives the number of vertical levels in the different domains. *Vertical levels (< 1000 m)* gives the number of vertical levels in the lowest 1000 m of the atmosphere. The lowest 21 model levels for all four domains are given in Table S.1. The time step (*dt*) and the *maximum slope angle* are given for simulations with 4 (14) smoothing cycles.

Domain	PBL mode	PBL scheme	SGS scheme	dx, dy (m)	Vertical levels	Vertical levels (< 1000 m)	dt (s)	Max. slope angle °
d01	~~mesoscale~~ non-LES	YSU[1]	1.5 order TKE[2] closure	1350	40	8	1 (6)	17.5 (9.9)
d02	LES	-	1.5 order TKE[2] closure	450	40	8	1/3 (2)	35.2 (26.5)
d03	LES	-	1.5 order TKE[2] closure	150	60	9	1/9 (1/2)	39.8 (36.8)
d04	LES	-	1.5 order TKE[2] closure	50	90	21	1/27 (1/4)	44.5 (37.4)

[1]YSU: Yonsei University PBL scheme, [2]TKE: Turbulent kinetic energy

complex terrain (Liu et al., 2011). Details about processes in the Morrison parameterization are given in Appendix A. An investigation of different microphysical parameterizations would be interesting, but is beyond the scope of this study. Given the high horizontal resolution no sub-grid parameterizations for cumulus clouds is used.

~~As initial and boundary conditions for the parent domain we use reanalysis of the~~ The 2.2 km horizontally resolved Consortium for Small-scale Modeling (COSMO–2) ~~model by MeteoSwiss~~ analysis by MeteoSwiss are used as initial and boundary conditions for the parent domain. For COSMO–2 ~~reanalysis~~ analysis data to be readable by the WRF pre-processing system a regridding of the rotated COSMO-coordinates to latitude-longitude coordinates is required. COSMO preprocessing, model adaptations and details about the model simulations are given in Gerber and Sharma (2018).

Topography in the model is based on the Aster Global Digital Elevation Model V002 with a resolution of one arc-second (METI/NASA, 2009). ~~Due~~ Terrain smoothing has been applied for all domains due to the very ~~complex~~ steep terrain in the simulation area~~, topography smoothing has been applied for all domains~~. Four cycles of the WRF 1–2–1 smoothing (i.e. a moving window filter with a window length of 3 and weights of 1:2:1 for the grid points i-1, i and i+1) ~~have to be applied to~~ are applied to all four domains to keep all slopes in ~~the 50-meter resolution domain~~ domain d04 (50 m horizontal grid spacing) below 45°. Additionally, the boundaries of the parent domain are smoothed to match COSMO-topography (Gerber and Sharma, 2018). Test simulations are run with 14 cycles of WRF 1–2–1 smoothing, which allows for a longer computational timestep and therefore saves computational time (Table 1). Maximum slope angles for all domains and different smoothing are given in Table 1. Simulations with different precision of topography further allow us to address the importance of the representation of topography in the model. To allow the simulations to adapt to higher resolution topography domains d01–d04 are run with a spin-up of ~~24h, 12h, 6h and one hour~~43 h, 19 h, 7 h and 1 h, respectively.

As the snow cover in complex alpine terrain is likely rougher than for a flat field and to account for non-resolved topography and additional smoothing, snow surface roughness length has been changed to 0.2 m. The chosen roughness length is much larger than roughness lengths assumed by e.g. Mott et al. (2015). However, grid spacing in our simulations is larger and the roughness length is chosen such that it accounts for roughness elements in complex terrain (e.g. large rocks) and non-resolved topography, which are assumed to have an average size of about 2 m. This estimate is based on a comparison of a ~~2-meter~~ 2-m digital terrain model (DTM-AV © 2018 swisstopo (5704 000 000)) to a ~~25 m~~ 25-m resolution digital elevation model (dhm25 © 2018 swisstopo (5740 000 000)), which reveals an average difference on the order of 2.5 ~~meters~~ m for bare ground conditions in domain d04 between 2200 and 2700 m asl. Hence, the estimate of 2 ~~meters~~ m is rather conservative but takes into account smoothing of the terrain by the snow cover.

For the model validation (Sect. 3.1) WRF variables are linearly interpolated to the coordinates of the meteorological station (see Sect. 2.2). Temperature is corrected for elevation due to ~~topographic~~ terrain smoothing using a moist-adiabatic temperature gradient of ~~$-0.0065 K m^{-1}$. As~~ $-0.0065\,\mathrm{K m^{-1}}$. Modeled wind speeds are extrapolated to the measurement height by applying a logarithmic wind profile, as wind measurements at the automatic weather stations are not taken at 10 ~~meters~~ m but 4 or 5 ~~meters~~ m above ground (Sect. 2.2)~~, wind speed is corrected for elevation by applying a logarithmic wind profile~~. This is a rough approximation given the assumption of a neutral atmosphere. For simulation domains d01–d03 ~~10-meter~~ 10-m wind speeds are ~~corrected~~extrapolated to the elevation of the sensor above the snow cover, while for domain d04 wind speeds at the lowest model level (approximately 3 ~~meters~~ m above ground) are used for the correction. The dynamic reference roughness length is chosen to be 0.2 m (corresponding to the surface roughness length in the model simulations). For wind direction comparisons wind directions at 10 ~~meter~~ m and 3 ~~meter~~ m above ground are chosen for the simulation domains d01–d03 and d04, respectively. As a reference COSMO–2 variables of the closest grid point to the station are included in the model validation and hence in Fig. 2 and Fig. 3. Two-meter temperature and ~~10-meter~~ 10-m wind speed of COSMO–2 are corrected for elevation by the same procedure as for the WRF simulations.

2.2 Automatic weather stations

Snow depth measurements from a total of 18 automatic weather stations in the ~~northwestern~~ central northern part of the ~~canton Grison (Figure~~ Grisons (Fig. 1) are used. Two stations, (*Dischma Moraine* and *Dischma Dürrboden*), were installed as part of the Dischma Experiment (DISCHMEX), in which processes of snow accumulation and ablation in the Dischma valley near Davos (Switzerland) are addressed (Gerber et al., 2017; Mott et al., 2017; Schlögl et al., submitted). 16 stations are part of the Intercantonal Measurement and Information System (IMIS). The 18 stations are located between 1560 m asl and 2725 m asl. The stations measure snow depth in addition to the standard meteorological parameters. All stations have ~~unshielded and unheated sensors. Biased temperatures during noon~~ shielded temperature and humidity sensors, but are unheated. Biased temperatures around midday and occasional data gaps due to iced instruments may therefore occur (Huwald et al., 2009; Grünewald et al., 2012). Two stations (*Dischma Moraine* and *FLU2*), which are located in the WRF domain with a horizontal grid spacing of 50 ~~m resolution WRF domain~~ m, are used for the model validation. The variables evaluated are ~~two-meter temperature, two-meter~~ 2-m temperature, 2-m relative humidity, wind speed and wind direction. Wind

measurements at IMIS stations are taken about 5 ~~meters~~ m above ground, while the wind sensor at station *Dischma Moraine* is located at about 4 ~~meters~~ m above ground.

2.3 Operational weather radar data

Weather radar datasets employed in the presented analyses are acquired by the MeteoSwiss operational radar located at the Weissfluhgipfel (2850 m asl), in the proximity of Davos. It is a dual-polarization Doppler weather radar, providing complementary information about the detected hydrometeors by considering their interaction with the incident electromagnetic radiation in both, horizontal and vertical, polarization planes. This complementary information leads to an enhanced clutter detection, which makes the radar measurements in such a complex mountainous terrain significantly more reliable. The polarimetry also makes it possible to identify the type of hydrometeors (Besic et al., 2016), which allows us to be confident that in the zone of interest for the presented study we deal with solid precipitation, consisting mostly of aggregates and crystals, and partly of rimed ice particles.

The radar operates in ~~5 minutes~~ 5-minutes cycles during which it scans the surrounding atmosphere by performing complete rotations at twenty different elevations, from $-0.2°$ to $40°$ (Germann et al., 2015). Operationally, the size of a radar sampling volume is 500 m in range, whereas the size observed in the perpendicular plane depends on the half-power beamwidth and increases with range. The acquired data undergo an elaborated procedure of corrections (Gabella et al., 2017). Before the quantity of precipitation at the ground level is estimated by averaging over 1 km~~^{2}~~ ^{2} the observations are corrected for the Vertical Profile of Reflectivity (VPR) with the weight assigned to volumes being inversely proportional to their height above the ground (Germann et al., 2006).

In the framework of our study, rather than relying on the operational radar product, we use data with the highest available resolution of 83 m in range. We also adopted a more conservative, non-operational method of clutter identification, which relies exclusively on the polarimetry and leaves very little residual clutter, however, sometimes at the expense of removing some precipitation. Given that we consider only radar measurements at low elevation angles in the vicinity of the radar and that the bright band is not present in our case studies (~~we observe~~ all radar measurements are from above 2800 m asl during the winter season), the observations are not corrected for the VPR. Furthermore, given the strong influence of wind on the snow precipitation, we restrict our precipitation estimate ~~on~~ to only four elevations, from the second to fifth $(0.4°, 1°, 1.6°, 2.5°)$, avoiding the ~~very~~ first one, judged to contain too little information due to the abundant rejected ground clutter areas.

Polarimetry helps to identify non-meteorological scatterers, to distinguish between different types of hydrometeors, to correct for signal attenuation and to make quantitative estimates of intense to heavy rainfall. For snowfall measurements it is common to use reflectivity Z at horizontal polarization and convert it into snow water equivalent S using a so-called Z-S relationship (Saltikoff et al., 2015):

$$Z = 100S^2. \tag{1}$$

The coefficients used in this formula account for the dielectric properties and fall velocities of snow and convert reflectivity Z in snow water equivalent S. The radar provides an indirect estimate of snowfall, rather than a direct measurement. Applied on each radar sampling volume scanned by the four selected elevations in the zone of interest (up to 40 km around the radar), the formula gives an estimate of liquid precipitation equivalent in the three-dimensional volume. By vertically averaging estimates from the four elevation sweeps using equal weights, we obtain the estimate of precipitation in polar (range, azimuth) coordinates at a flat plane at the height level of the radar. These estimates are summed up over ~~24h~~ 24 h to get the accumulation maps used in the study.

Further on, the polar accumulation maps are re-sampled by means of the bi-linear interpolation to the Cartesian grid of the regional domain (450 m resolution) and the local domain (300 m resolution). The obtained Cartesian maps are finally processed to remove the residual clutter using a 3×3 median filter, partly or entirely. The former means that only the isolated high values in the original map are replaced with the corresponding value of the filtered map, at the positions where the difference between the original and the filtered map appears to be larger than 5 mm (hereafter "partly-filtered"). The latter means that the entire map is influenced by the median filtering (~~denoted by "Radar all filtered" in the figures in the results~~hereafter denoted as "entirely-filtered").

2.4 Autocorrelation and variogram analysis

To investigate the variability of snow precipitation and accumulation patterns and their relation to topography a scale analysis, based on 2-dimensional (2D) autocorrelation maps and variograms, is performed. 2D-autocorrelation maps and variograms are further used to relate variability in radar and WRF precipitation. Given the resolution restriction by the radar measurements (Sect. 2.3) we analyze ~~three~~ two different domains using horizontal resolutions of 450 m ~~,~~ and 300 ~~m, 150 m and 50~~ m, respectively. The domain with a resolution of 450 m covers ~~about 30 km surrounding~~ an area of about 58 km times 56 km centered over the radar on Weissfluhgipfel (hereafter regional domain, ~~Figure~~ Fig. 1). The domain with a resolution of 300 m covers an area of 24 km times 21 km to the south of Davos (Switzerland) including the Dischma valley (hereafter local domain). Radar data (300 m resolution) and WRF precipitation on ~~all resolutions~~ three resolutions (450 m, 150 m and 50 m) are additionally, evaluated on domain Dischma to address the influence on the spatial resolution of variability. Domain Dischma covers the upper Dischma valley with an extent of 9 km times 9 km.

~~The~~ To produce variograms the semivariance (γ) is calculated at 50 logarithmic lag distance bins (h~~) is calculated~~ , i.e. a set of distance ranges) by

$$\hat{\gamma(h)} = \frac{1}{2|N(h)|} \sum_{(i,j)\in S(h)} (a_j - a_i)^2, \tag{2}$$

where $S(h)$ are the point pairs (i,j) and $N(h)$ gives the number of point pairs of the evaluated variable a. WRF and radar snow precipitation and topography are evaluated at 450 m and 300 m resolutions with a maximum lag distances of 25 km and 10 km, respectively. Variograms for domain Dischma are calculated with a maximum lag distance of 5 km. Minimum numbers of point pairs in one lag distance bin for the local and regional domain are 18317 and 8035, respectively. For domain Dischma the minimum number of point pairs is between 677 and 55419, depending on the resolution.

To determine scaling properties an empirical log-linear model is fit to the variogram by least square optimization (Schirmer et al., 2011). The model used is not a valid variogram model but used to describe the experimental variograms and chosen to be consistent with Schirmer et al. (e.g. 2011). For all variograms three empirical log-linear models are fit:

$$y(x) = \begin{cases} \alpha_1 * \log(h) + \beta_1, & \text{for } \log(h) < l_1 \\ \alpha_2 * \log(h) + \beta_2, & \text{for } l_1 \geq \log(h) < l_2 \\ \alpha_3 * \log(h) + \beta_3, & \text{for } \log(h) \geq l_2 \end{cases} \quad (3)$$

using the constraint that each log-linear model needs to contain a minimum of four data points and the continuity constraint(s)

$$\begin{aligned} \alpha_1 \log(l1) + \beta_1 &= \alpha_2 \log(l1) + \beta_2 \\ \alpha_2 \log(l2) + \beta_2 &= \alpha_3 \log(l2) + \beta_3, \end{aligned} \quad (4)$$

where $\alpha_{1,2,3}$ and $\beta_{1,2,3}$ are the slopes and intercepts of the three log-linear models, respectively. Scale breaks (l_1, l_2) are the lag distances of the intersections of the first and second, and second and third log-linear model, respectively. Scale breaks were previously found to determine the scale of a change of dominant processes (e.g. Deems et al., 2006). To address the variability with respect to the overall variability ~~of values~~in the respective domain, all variograms are normalized by the total domain-wide variance.

2D-autocorrelation is calculated based on Pearson's correlation coefficient r of all grid point pairs for a maximum lag distance of ± 40 grid points in x- and y-direction. This results in maximum lag-distances of 18 km for the regional domain.

2.5 Snowfall events

This study is based on three precipitation events in winter 2016. On 31 January 2016 the Azores high and a low-pressure area over Scandinavia induce westerly flow over central Europe and relatively mild temperatures with about ~~−3°C~~ −3°C at 2500 m asl. A shift of the Azores high toward northern Spain and a trough over eastern Europe lead to a change in wind direction toward northerly advection and a decrease of temperature (about ~~−12°C~~ −12°C at 2500 m asl) on 4 February 2016. On 5 March 2016 a low-pressure area over France, which is part of a large depression area over central Europe, causes southerly advection over Switzerland. Temperatures are about ~~−7°C~~ −7°C at 2500 m asl. Given the relatively high temperatures on 31 January 2016, which resulted in quite substantial liquid precipitation ~~on~~ at the lowest elevations, total (solid and liquid) ground precipitation is evaluated. This does not make a big difference for the precipitation events on 4 February 2016 and 5 March 2016 but is essential for the precipitation event on 31 January 2016. For precipitation patterns at the elevation of the radar (2830 m asl) we only analyze solid precipitation from WRF.

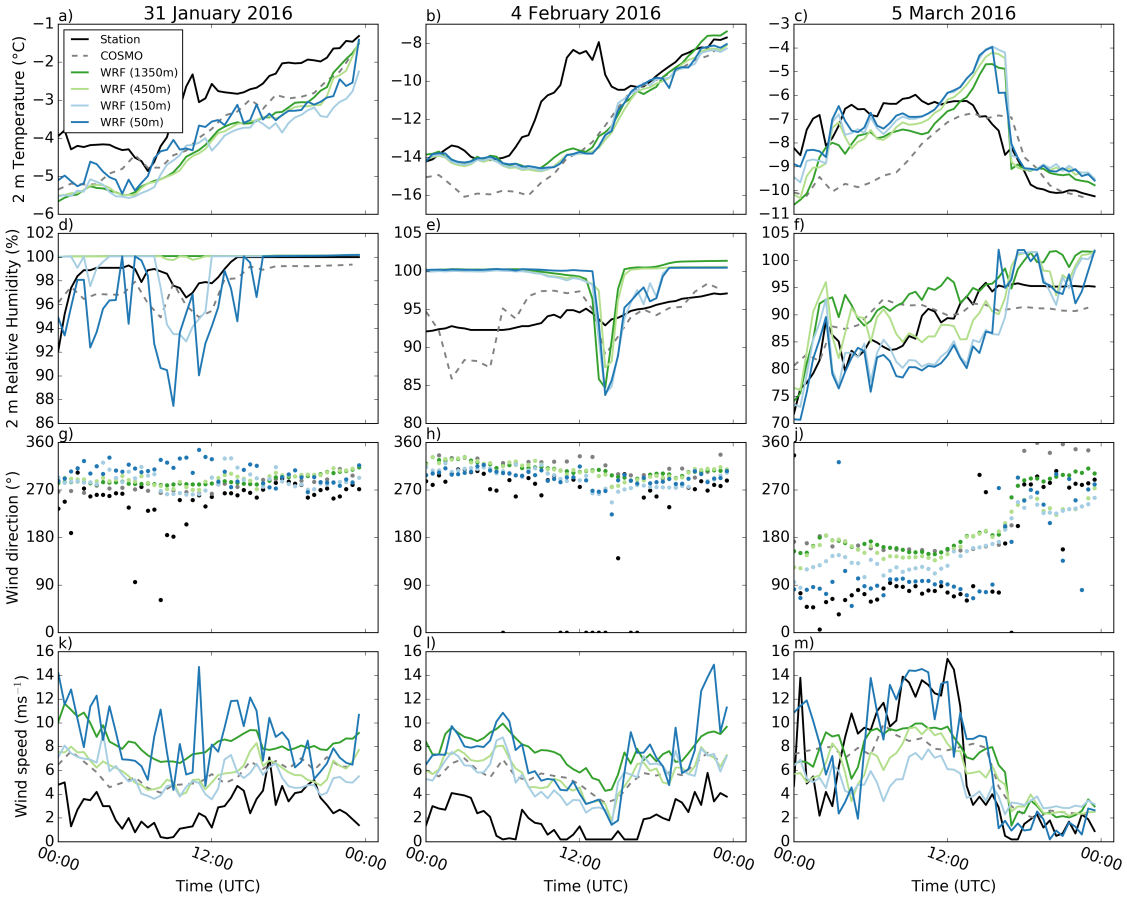

Figure 2. Comparison of ~~two-meter~~ 2-m temperature (C°), ~~two-meter~~ 2-m relative humidity (%), ~~4-meter~~ 4-m wind speed (~~$m.s^{-1}$~~ ms^{-1}) and wind direction (°) at station *Dischma Moraine* (black) to WRF simulations interpolated to the coordinates of station *Dischma Moraine* for the three precipitation events on 31 January 2016, 4 February 2016 and 5 March 2016 for all four simulation domains (d01: ~~blue~~dark green, d02: ~~red~~light green, d03: ~~cyan~~light blue, d04: ~~magenta~~dark blue). For comparison COSMO–2 is added for the closest grid point (dashed gray). Two-meter temperature in WRF and COSMO are corrected for elevation based on a moist-adiabatic temperature gradient.

3 Results and Discussion

3.1 Point validation of WRF simulations

Two-meter air temperature, and 4- or ~~5-meter~~ 5-m wind speed and direction at two stations (Sect. 2.2) are compared to WRF to validate the model (~~Figure 2and Figure 3~~Fig. 2a-c and Fig. 3a-c). For ~~all stations two-meter temperature matches well with~~

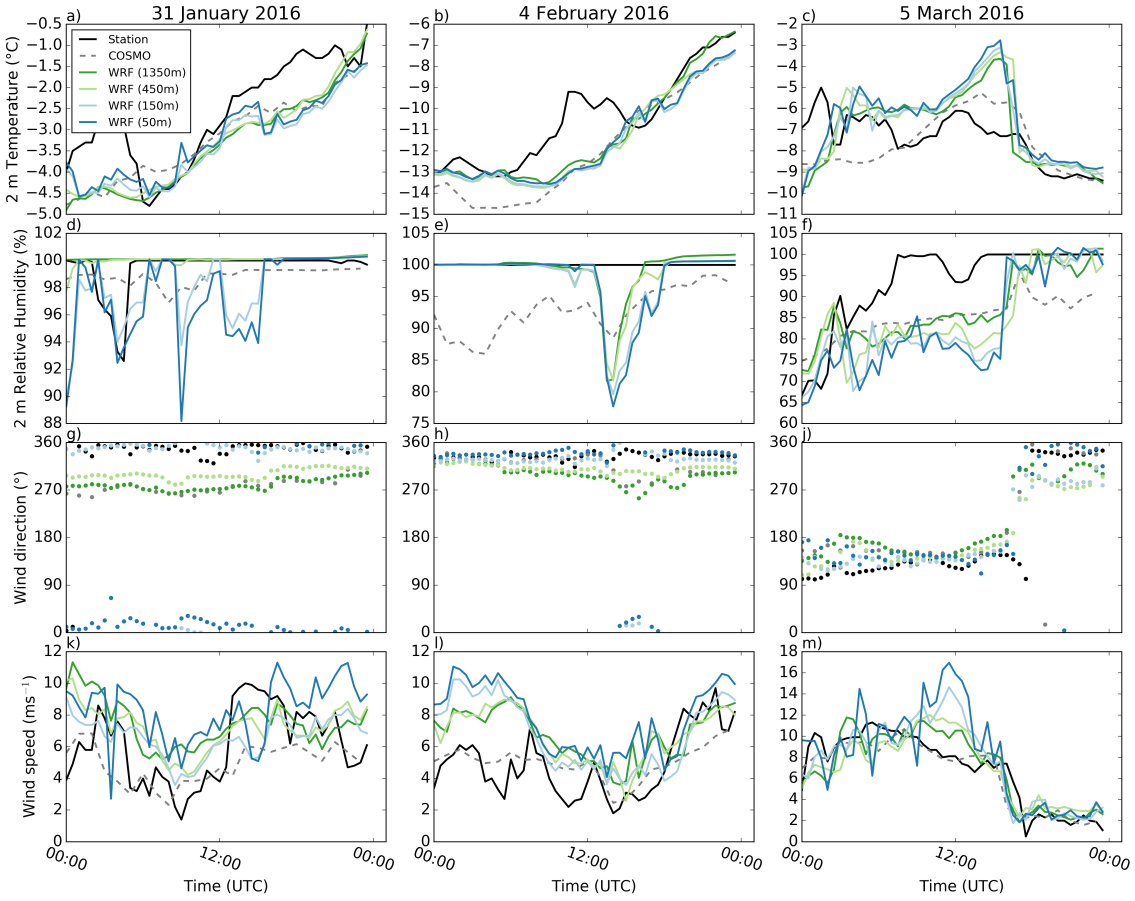

Figure 3. As ~~Figure~~ Fig. 2 but for the station *FLU2* on the Flüelapass with ~~5-meter~~ 5-m wind speed and direction.

~~observations~~ both stations 2-m temperature matches reasonably with observations although especially for the precipitation event on 4 February 2016 substantial temperature deviations occur around midday. Deviations of the WRF model from station measurements during midday are likely ~~due to~~ caused by errors in station measurements due to radiative heating of the multiplate shielded temperature sensors (Huwald et al., 2009, Sect. 2.2). Additionally, offsets in ~~temperature are~~ simulated temperatures may be linked to offsets in the input by COSMO–2.

Relative humidity shows partially good agreement, but shows a strong temporal variability (Fig. 2d-f and Fig. 3d-f). Some disagreement of relative humidity simulated by WRF compared to station measurements ~~is likely~~ might be induced by COSMO input, which for some cases shows an offset compared to station measurements. This bias can sometimes be reduced by WRF simulations but for other cases WRF introduces an additional bias. WRF is generally able to capture main drops in relative hu-

midity at ~~stations,~~ the two investigated stations but it introduces additional drops compared to measurements. The ~~introduction of drops~~ microphysics parameterization is originally developed for simulations with a coarser resolution, which produce less vertical motions. Thus, the introduction of a higher variability in relative humidity ~~by WRF~~ in our WRF simulations may be due to strong subsidence and lifting, which lead to an overestimation of ~~subsidence in the model~~adiabatic cooling or warming and hence to an overestimation of humidity generation or decay. Additionally, differences between modeled and measured relative humidity may be due to measurement uncertainties.

Simulated wind direction shows ~~very~~ good agreement with measured wind direction (Fig. 2g-i and Fig. 3g-i). In complex terrain, simulations are often limited to resolutions, which are too coarse to resolve ~~smaller scale~~ smaller-scale terrain features that affect near-surface wind direction (e.g. due to a lack of high resolution terrain data, or computational resources), and thus cannot accurately capture changes in wind direction close to the surface where weather stations are located. Good agreement in wind direction modeling in our COSMO–WRF simulations in complex terrain is likely due to the high resolution of topography. For some ~~stations additional improvement of wind direction comparisons is visible~~ cases wind directions in the WRF simulations additionally improve for higher resolutions although for others terrain smoothing is likely to have adverse effects on modeled wind direction.

Compared to the good agreement of wind direction, wind speeds show only partially good agreement with station measurements (Fig. 2k-m and Fig. 3k-m). Wind speeds were found to strongly depend on the subgrid-scale turbulence parameterization and a strong overestimation of wind speeds was observed for different simulation setups (not shown). Applying the improved non-linear subgrid-scale turbulence parameterizations (Mirocha et al., 2010, 2014) leads to instabilities in the current model setup. The use of a snow surface roughness length of 0.2 m, representing the combined roughness of snow and surface features (e.g. ~~rocks),~~ boulders and rocky outcroppings, Sect. 2.1), compared to simulations with standard WRF roughness length of snow of 0.002 m, could partially reduce overestimated wind speeds ~~. For some stations and dates an overestimation of wind speed is already observed in COSMO–2, which is the most likely reason for wind speed overestimation at these stations. Additional reasons for an overestimation of wind speeds may be manifold. Strong wind speeds due to speed up in ridge areas~~ (Gerber and Sharma, 2018). While we address non-resolved topography based on an increased snow surface roughness length, another approach to improve wind speeds in WRF simulations has been introduced by Jiménez and Dudhia (2012), who use a sink term in the momentum equation based on subgrid-scale topography. They demonstrate the ability of their approach to improve surface wind speeds. However, with this approach, the effect of the subgrid scale topography is only included for simulations using a PBL parameterization. As in our model setup a PBL parameterization is only applied for domain d01, we address the non-resolved topography by increasing the surface roughness, which allows us to include the effect of non-resolved topography for all four simulation domains. In addition, our simulations are run over snow covered terrain, which implies that the standard roughness length for snow used in WRF (on the order of 10^{-3} m) is two orders of magnitude lower than roughness lengths representative of the scale of complex terrain in our simulations (on the order of 10^{-1} m). Applying the PBL version of Jiménez and Dudhia (2012) might be a possibility to reduce excess wind speeds in domain d01, which might also impact wind speeds in the domains d02–d04. However, such a sensitivity study is out of scope of the present investigation.

Based on our approach COSMO–WRF still simulates excess wind speeds for the two precipitation events on 31 January 2016 and 4 February 2016. This overestimation is assumed to be connected to the upwind location of both stations during these two precipitation events, as speed up over windward slopes and ridges are a known problem ~~for model simulations (Gómez-Navarro et al., 2015). Therefore~~(Mott et al., 2010; Gómez-Navarro et al., 2015). Hence, the exact location of the station relative to the ridge is important to verify wind speeds.

~~As an example, station *Dischma Moraine*~~ Furthermore, local terrain features upstream of the station may disturb the wind field. For example station Dischma Moraine is located on a moraine on the northern side of the ridge between Piz Grialetsch and Scalettahorn. Station ~~*FLU2*~~ FLU2 is located on the northern side of Flüelapass above a small rock face and to the east of a terrain knoll. ~~Due to the resolution and additional terrain smoothing the small-scale features(moraine, small rock face and terrain knoll) are~~ Such terrain features, while not represented in ~~WRF topography even at 50 m resolution. Such small-scale features introduce very local flow features and may either induce local speed-up effects or can reduce wind speedsdue to enhanced roughness~~the model, may strongly reduce wind speeds in reality. For station Dischma Moraine on the 31 January 2016 and the 4 February 2016 an overestimation of wind speed is already observed in COSMO–2, which might be an additional reason for wind speed overestimation at this station. However, given the fetch distances and spin-up times of our model simulations (Sect. 2.1), we expect the atmosphere to develop independently. Still, if COSMO wind speeds are constantly overestimated WRF may not be able to correct for excess wind speeds. Station measurements are also prone to measurement uncertainties and riming of the unheated instruments may lead to an underestimation of wind speeds (Grünewald et al., 2012).

Generally, reasons for an overestimation of wind speeds may be manifold. An exact estimation of wind speeds at stations in the model is ~~therefore not expected from the model and~~ not expected due to unresolved topographical features in the complex terrain of our study site. An additional source of uncertainty – though unlikely to be on the order of the strong excess wind speeds – is the extrapolation of wind speeds based on the assumption of a neutral atmosphere. While different potential causes of wind speed overestimation are discussed above, actual reasons for deviations ~~may be manifold~~in wind speed remain unknown.

Overall, we show that the presented simulation setup reasonably captures temperature, relative humidity and wind conditions in complex terrain at two stations. Wind speeds on the windward side of the mountain ridges tend to be overestimated. Temperature deviations around midday are likely due to measurement uncertainties.

3.2 Spatial snow precipitation and accumulation patterns

~~Overall, radar~~ Radar precipitation maps of the regional domain covering ~~about 30 km surrounding~~ an area of about 58 km times 56 km centered over the radar on Weissfluhgipfel (~~Figure~~ Fig. 1) tend to show wind direction (~~Figure 2, Figure 3and Figure~~ Fig. 2g-i, Fig. 3g-i and Fig. 4d-f) dependent precipitation patterns (~~Figure~~ Fig. 4). ~~A strong south-north gradient in precipitation is observed for precipitation~~ The precipitation field on 31 January 2016 ~~, while precipitation~~ shows a strong south-north gradient (Fig. 4a), while the precipitation field on 4 February 2016 shows a more homogeneous distribution (Fig. 4b). For the precipitation event on 5 March 2016 radar precipitation maxima are observed over the mountain ridges in the southern part of the domain (Fig. 4c). Although our regional domain ~~is located within the Alps~~does not represent a cross

section across the whole alpine mountain range, a north-south ~~gradient in precipitation for southerly advection and a (~~south-north~~gradient for northerly advection are~~) precipitation gradient for southerly (northerly) advection are apparent. This is in good agreement with large-scale orographic precipitation enhancement (Houze, 2012; Stoelinga et al., 2013), which favors precipitation on the upwind side of a mountain range due to topographically induced lifting and a drying due to sinking air masses downwind of the mountain range.

These large-scale patterns of orographic ~~enhancement of precipitation~~ precipitation enhancement are partially captured in the WRF simulations (~~Figure 4~~Fig. 4d-f). Especially, for southerly advection (precipitation event on 5 March 2016) this large-scale effect is well represented in COSMO–WRF, where precipitation maxima occur over ~~terrain~~ mountain ridges in the southern part of the domain and a ~~south-north~~ north-south precipitation gradient is present. For northerly to north-westerly advection (precipitation events on 31 January 2016 and 4 February 2016), however, snow precipitation maxima in the WRF simulations are shifted eastward compared to radar precipitation estimates, i.e. toward the outflow boundary~~, in the model compared to radar estimations. Based on this visual comparison for all three events we hypothesize that both, radar and WRF precipitation patterns are driven by wind direction and topography.~~ .

~~Disagreement of patterns may be connected to the strong smoothing of topography. Additionally, microphysics~~ Microphysics and precipitation dynamics in the model are likely to be a limiting factor in terms of small-scale precipitation patterns. Disagreement between radar and WRF precipitation patterns may further be connected to the strong terrain smoothing in the model. Despite of the high resolution of our simulations, slope angles are relatively low with maximum slope angles of ~~of~~ 35.2° in the regional domain due to the application of ~~topographic~~ terrain smoothing (Table 1). Given even ~~flatter slopes~~ lower slope angles in domain d01 precipitation fed to domain d02 may already be too weak and thus needs to develop within domain d02. As mountains in the north-western part of the domain are shallower than mountains in the south-eastern area (Fig. 1), lifting condensation may not be strong enough in the north-western area of the domain, leading to precipitation generation further downstream in the domain, where steeper and higher mountains may even lead to too strong precipitation enhancement. Additionally, if the tendency of ~~an overestimation of wind speeds~~ overestimated wind speeds sustains up to higher atmospheric levels in the model, this may lead to an overestimation of the advection of hydrometeors in the microphysics scheme (Morrison et al., 2005)~~, which may~~ . This would result in a downstream shift of the precipitation maximum. However, we do not expect this to have a strong impact on the regional scale precipitation distribution. Thus, there are likely additional reasons for the observed downstream shift of WRF precipitation compared to radar precipitation, which remain difficult to explain.

On a mountain-valley scale (local domain) the same tendencies emerge with good agreement in overall gradients for southerly advection and partially reversed gradients for northerly to north-westerly advection when comparing WRF to radar precipitation patterns (not shown). WRF precipitation patterns generally show a stronger ~~dependence to~~ dependency on topography expressed in ~~an elevation gradient~~higher precipitation rates over higher elevations. Radar precipitation patterns additionally reveal small-scale precipitation patterns. Very small-scale patterns are visible on the ~~partially filtered~~ partly-filtered radar maps (Sect. 2.3, not shown), while in ~~median-filtered radar estimations (Figure~~ entirely-filtered radar estimates (Fig. 4a-c) ~~smallest scale~~ smallest-scale patterns are eliminated but patterns of about 1 km size emerge. Patterns in the ~~median-filtered~~

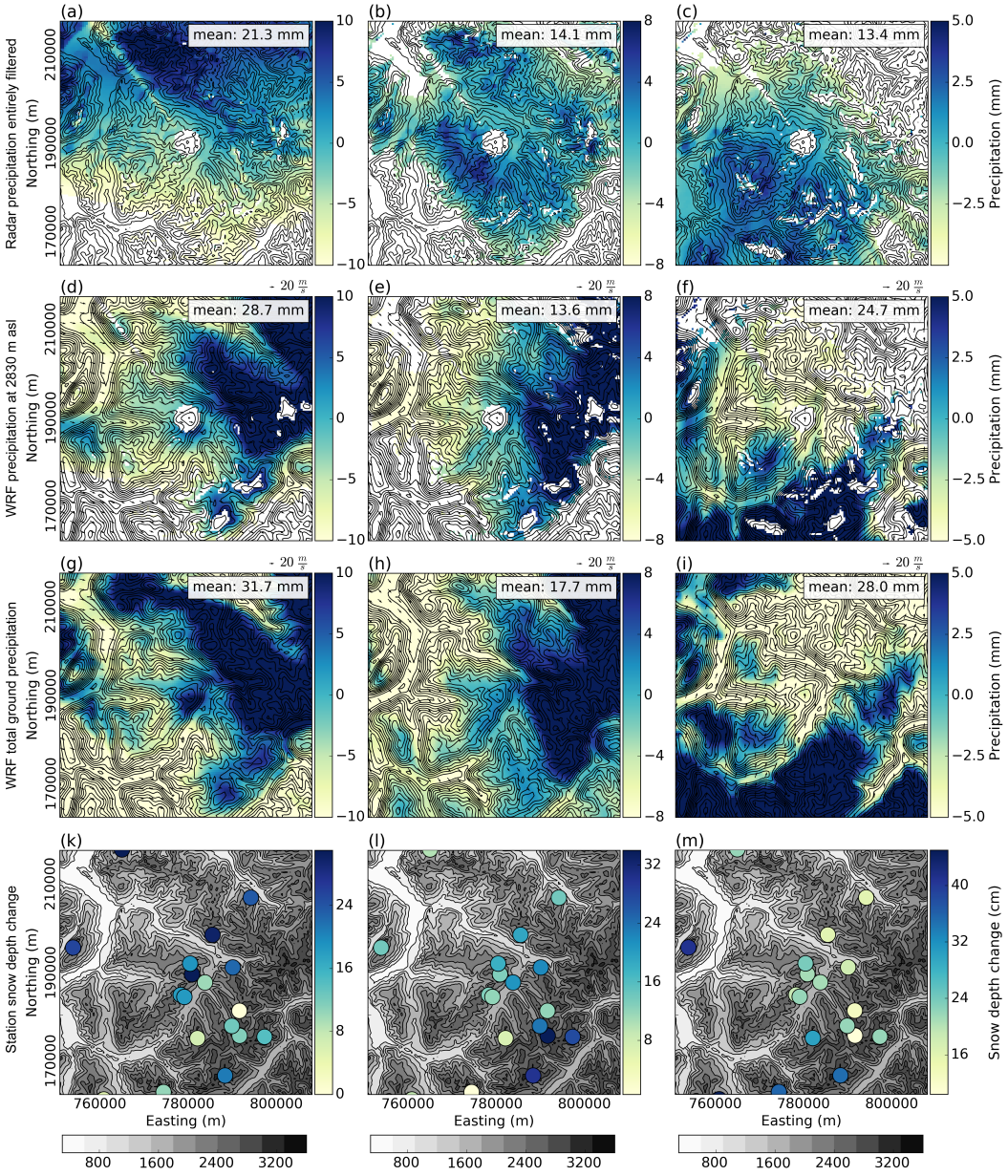

Figure 4. Twenty-four hour snow precipitation (mm) from a-c) MeteoSwiss ~~filtered~~ entirely-filtered radar measurements, d-f) Weather Research and Forecasting (WRF) snow precipitation at 2830 m above sea level (m asl), g-i) WRF total ground precipitation and k-m) 24 h snow depth changes (cm) at meteorological stations on 31 January 2016 (left), 4 February 2016 (middle) and 5 March 2016 (right) with a resolution of 450 m in the regional domain (~~Figure~~ Fig. 1). Radar precipitation is estimated from different radar elevations (Sect. 2.3). White areas in a-f mark areas where clutter is removed and small values in the radar data are masked. The same mask is applied for WRF solid precipitation at 2830 m asl (approximate elevation of the radar, d-f), for which additionally areas where WRF topography is higher than 2830 m asl are masked. Arrows in d-f indicate wind direction and speed at an elevation of 2830 m asl. Northing and easting are given in the swiss coordinate system (CH1903LV03). Note different colorbars. Contour lines in a-c) and k-m): dhm25 (c) 2018 swisstopo (5740 000 000). Gray shading in k-m) represent topography.

entirely-filtered data could be small-scale precipitation cells, while the very small-scale patters are most likely noise in the radar data (see Sect. 3.4).

~~The depth of new snow~~ New snow depth measured at 18 automatic weather stations in the regional domain (~~Figure~~ Fig. 4k-m) over 24 hours shows a distinct elevation gradient, which is quite well represented by WRF total ground precipitation (~~Figure~~ Fig. 4g-i). For 31 January 2016 and 5 March 2016 the ~~large scale~~ large-scale precipitation trend observed in the radar data is generally represented in station measurements. On 4 February 2016 station measurements suggest a precipitation peak in the upper Dischma valley (lower left quadrant in ~~Figure~~ Fig. 4l), which agrees with WRF simulations. Radar ~~estimations~~estimates, however, show a more homogeneous distribution of precipitation on 4 February 2016. Snow depth changes at the stations are very local and strongly affected by wind redistribution of snow, which may disturb the large-scale gradient. Additionally, the distribution of stations is not homogeneous over the regional domain and fewer stations are available in the western part of the domain.

The visual comparison of radar and WRF precipitation patterns for all three events (Fig. 4) reveals that precipitation patterns are influenced by wind direction and topography. Large-scale precipitation patterns are in agreement with station measurements, although the latter are strongly influenced by the local wind field and snow redistribution processes.

3.3 Mean variability

Radar precipitation ~~distribution~~ distributions at 2830 m asl on the regional domain (450 m resolution~~) shows~~ , Fig. 5) show a larger interquartile range (IQR) than radar precipitation on the local domain (300 m resolution, Supplementary Information S2), confirming that local precipitation is more uniform than regional precipitation~~(Figure 5). Median precipitation in the local domain depends strongly on the large-scale precipitation distribution (Figure 4), i.e. a higher median if the large-scale precipitation distribution is such that~~ . Radar median precipitation over 24 h is on the order of 10 to 20 mm water equivalent for all three precipitation events in the regional domain. The median of radar precipitation in the local domain ~~is strong.~~

can be both, higher or lower than in the regional domain. Although radar estimates are based on a reference S-Z relationship, the employed formula (Eq. 1) is not immune to potential estimation errors. Therefore, despite reasonably assuming that the potential estimation errors should not significantly influence the variability and the relative intensity of the precipitation fields, we consider potential inaccuracies in our interpretations.

~~Even though main precipitation areas for the two snowfall~~ For the precipitation events on 31 January 2016 and 4 February 2016 ~~are shifted toward the outflow boundaries of the radar domain, spatial median precipitation~~ median precipitation at 2830 m asl in the COSMO–WRF simulations is in reasonable agreement with radar median precipitation (~~Figure 5).~~ Fig. 5), even though WRF and radar precipitation patterns are different (Sect. 3.2). However, for the precipitation event on 5 March 2016 the median of precipitation in the regional domain is higher in WRF simulations compared to radar measurements~~even though~~ , while the large-scale precipitation gradient is in good agreement ~~.~~ (Fig. 4c and Fig. 4f). The IQR of ~~precipitation for this event is matching better with~~ WRF precipitation is generally larger compared to the IQR of radar precipitation ~~, but the precipitation distributions in WRF simulations have longer tails .~~ and the domain-wide WRF precipitation distribution has longer tails compared to the radar precipitation distribution. These tendencies are even stronger for the domain-wide WRF

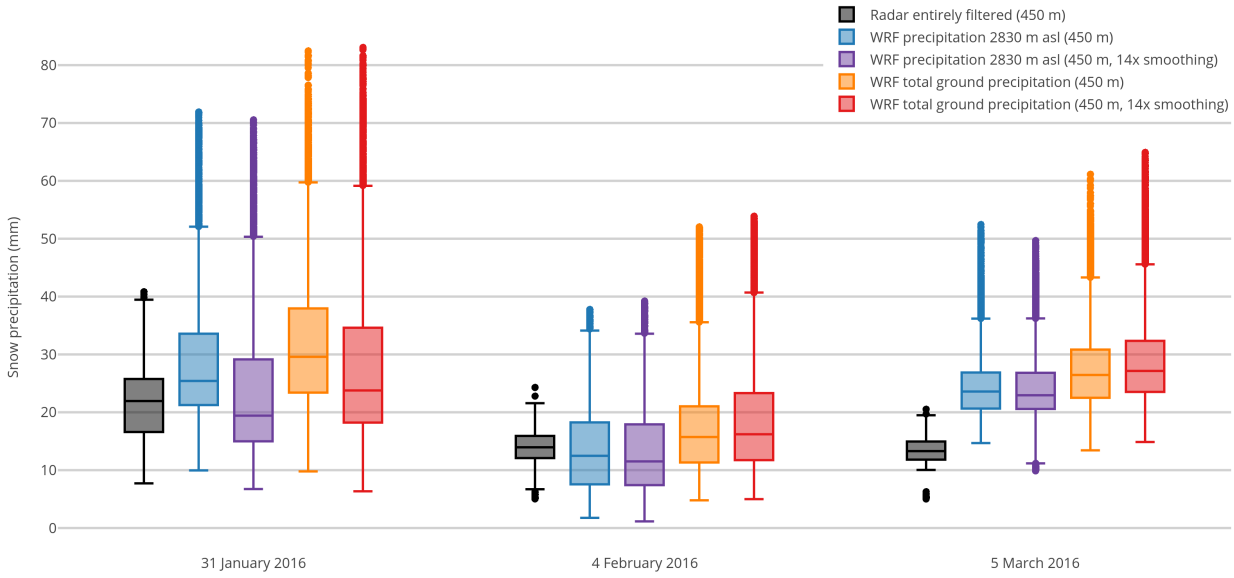

Figure 5. Domain-wide 24 h precipitation statistics for the regional domain (450 m resolution, ~~light colors) and local (300 m resolution, dark colors) domain (Figure~~ Fig. 1) for the three precipitation events on 31 January 2016, 4 February 2016 and 5 March 2016. Gray colors show ~~filtered~~ entirely-filtered radar precipitation. WRF precipitation at 2830 m above sea level (m asl) for simulations with weak terrain smoothing (Sect. 2.1) and strong terrain smoothing are given in blue and violet, respectively. Orange (red) shows boxplots of WRF total ground precipitation for weak (strong) terrain smoothing. Radar precipitation and WRF precipitation at 2830 m asl are masked (as shown in ~~Figure~~ Fig. 4).

precipitation distribution on the local domain (Supplementary Information S2). This confirms the hypothesis that the model tends to overestimate precipitation for higher resolutions with steeper and more complex topography.

The domain-wide median and IQR of precipitation at ~~radar elevation~~ 2830 m asl in WRF simulations with weaker terrain smoothing and stronger terrain smoothing (Sect. 2.1) are similar with a slight tendency of higher median values for weaker smoothing, indicating that the accuracy of topography does not have a strong influence on the domain-wide statistics of precipitation on the regional scale. Enhanced precipitation for weaker terrain smoothing compared to stronger terrain smoothing could be explained by enhanced precipitation production due to steeper topography. ~~On the local domain (300 m resolution) differences between medians in WRF and radar estimations tend to be larger compared to differences on the regional domain, which supports the hypothesis that the model tends to overestimate precipitation for higher resolution with steeper and more complex topography.~~

An overestimation of precipitation in WRF simulations was previously reported ~~(e.g. Leung and Qian, 2003; Mass et al., 2002; Silverma~~ could be due to various reasons. ~~Leung and Qian (2003), Mass et al. (2002)~~ Mass et al. (2002) and Leung and Qian (2003) among others report that WRF tends to show a stronger overestimation of precipitation for higher model resolutions ~~but also find~~ compared to coarser model resolutions. Additionally, they document a dependency on the intensity of precipitation. An overestimation of orographic ~~enhancement of precipitation~~ precipitation enhancement in more complex terrain or an overestimation of moisture in the model were further reported by Silverman et al. (2013). An overestimation of orographic precipitation enhancement would be in agreement with a stronger overestimation of precipitation for the local domain compared to the regional domain and for weaker smoothing compared to stronger smoothing. Furthermore, it is likely to occur for simulations with high horizontal ~~resolutions~~ resolution as higher peaks and steeper slopes are preserved (Silverman et al., 2013). ~~Higher~~ Compared to a shallow topography, higher peaks and steeper slopes may cause stronger lifting and subsidence, which is also a likely cause for additional drops in relative humidity in WRF compared to measured relative humidity (Sect. 3.1, ~~Figures 2 and~~ Fig. 2 and Fig. 3). ~~However, this~~ This tendency seems to ~~be only represented at~~ only apply for the highest elevations~~, while at~~ . For lower elevations strong smoothing may ~~not allow~~ result in elevation differences, which are too small for precipitation to evolve by lifting condensation (Sect. 3.2). As additional reasons for precipitation overestimation in WRF an overestimation of precipitation in the driving model (Caldwell et al., 2009) and underlying landuse characteristics (Silverman et al., 2013) were mentioned. The latter was, however, previously found to only have a weak influence on the precipitation amount (Pohl, 2011). Humidity in COSMO–2 is an unlikely reason as COSMO–2 ~~show~~ shows rather a tendency of underestimating relative ~~humiditiy~~ humidity compared to station measurements (~~Figures 2 and~~ Fig. 2 and Fig. 3). Even though there are many possible reasons for overestimation of precipitation in WRF, the estimation of solid precipitation from radar measurements is also subject to uncertainties (e.g. Cooper et al., 2017). Given uncertainties in radar precipitation ~~estimations~~ estimates the comparison of median domain-wide precipitation should be taken with care. An in depth analysis of spatial variabilities is given in Sect. 3.4.

~~WRF snow precipitation at~~ At the ground level WRF precipitation tends to show higher median values of precipitation compared to WRF precipitation at ~~radar elevation~~ 2830 m asl for both domains. The IQR is similar. From this we hypothesize that there are precipitation formation or enhancement processes taking place between the elevation of the radar and the ground. This is in good agreement with the fact that near-surface processes can strongly enhance snow precipitation (e.g. riming). Overall, this analysis shows that WRF tends to overestimate domain-wide precipitation and precipitation variability at 2830 m asl compared to radar estimates.

3.4 Spatial variability

To address spatial patterns and variability of precipitation a scale analysis is performed augmented with a 2D-autocorrelation analysis (Sect. 2.4). Given the overestimation of precipitation in the model and the large differences in domain-wide variability between the model and radar precipitation ~~estimations~~ estimates (Sect. 3.3), all variograms are ~~shown as normalized variograms~~normalized by the domain-wide variability, which allows analysis of spatial patterns with respect to the overall range of precipitation values. From the analysis of precipitation patterns (Sect. 3.2), we further know that there are strong

large-scale precipitation gradients in the regional domain. ~~Due to large-scale gradients, small and intermediate scale structures in~~ In the variogram analysis small- and intermediate-scale structures may be hidden by the large-scale gradient. To avoid this and non-stationarity of patterns, we first present variograms of detrended precipitation fields ~~are presented~~ (Sect. 3.4.2). However, to assess processes acting at different scales, variograms of non-detrended precipitation patterns are ~~also~~ subsequently analyzed in a scale analysis (Sect. 3.4.3). Finally, a 2D-autocorrelation analysis is used to comment on directional dependencies of precipitation patterns (Sect. 3.4.4).

3.4.1 Large-scale precipitation trends

Large-scale precipitation patterns show a strong gradient ~~of precipitation (Figure~~ (Fig. 4). Therefore a ~~linear trend is fit~~ plane is fit linearly to the precipitation fields describing the large-scale precipitation trend (Table 2). The trend on the 31 January 2016 roughly points toward the North. For the precipitation event on 5 March 2016 the trend points roughly to the South. Given a southerly advection on 5 March 2016 this direction corresponds to the main wind direction and therefore agrees with the theory of large-scale orographic precipitation enhancement or rather the drying trend due to sinking air further downstream within the mountain range. The ~~north-south~~ south-north gradient on 31 January 2016 roughly agrees with the main wind direction but points out that regional trends of ~~larger scale~~ larger-scale patterns may not exactly be aligned with wind direction. For the precipitation event on 4 February 2016 the intensity of the trend (i.e. the strength of inclination of the linearly fitted plane) is, however, ~~very~~ weak and therefore the ~~direction~~ orientation of the slope is arbitrary. For this day, we hypothesize that either dynamics were more variable preventing the evolution of a strong gradient or lifting condensation due to the orography was not as efficient as for the other two events. For two events (31 January 2016 and 4 February 2016) the model has trouble reproducing the trend (i.e. orientation and intensity of the linearly fitted plane). For 31 January 2016 the deviation of orientation between the trends of radar precipitation and WRF precipitation at 2830 m asl is about 70° but with a similar intensity of the trend. For 4 February 2016 the model shows a strong trend of precipitation, while the intensity of the trend is ~~very~~ weak in the ~~filtered~~ entirely-filtered radar data. However, for the precipitation event on 5 March 2016 the trend is reasonably captured by the model with a deviation of the ~~direction~~ orientation of 16.6° and a slightly stronger intensity of the trend in the model compared to the radar estimation.

Disagreement in precipitation patterns, trend ~~direction~~ orientation and intensity on 4 February 2016 (quite homogeneous precipitation distribution in the radar ~~estimation (Figure~~ estimate (Fig. 4) compared to the strong downstream shift of precipitation in WRF) and the overestimation of precipitation in the model give evidence for a too ~~idealistic~~ simplistic representation of precipitation in the model (i.e. simplified microphysics and ~~particle~~ cloud dynamics), which tends to overestimate the effect of highest topographic features but misses precipitation over shallower areas. Good agreement in the intensity of the trend on 31 January 2016 and good agreement of the ~~direction~~ orientation of the trend on 5 March 2016, however, show that the model is able to capture large-scale precipitation trends, which may be connected to a large-scale orographic enhancement.

Table 2. Large-scale linear trends of entirely-filtered radar and WRF precipitation patterns on the regional domain (~~Figure~~ Fig. 1). WRF precip. at 2830 m asl refers to solid precipitation in WRF simulations at 2830 m above sea level and WRF total ground precip. refers to the total (solid and liquid) precipitation at the ground level. *Orientation* gives the direction of the slope and *Intensity* the strength of inclination. 0° would indicate a slope pointing toward the East. WRF snow precipitation is from simulations with weak terrain smoothing (Sect. 2.1).

	31 January 2016		4 February 2016		5 March 2016	
	Orientation	Intensity	Orientation	Intensity	Orientation	Intensity
Radar entirely filtered	86.9°	0.17	-125.9°	0.01	-114.8°	0.04
WRF precip. at 2830 m asl	16.7°	0.22	-5.1°	0.21	-98.2°	0.12
WRF total ground precip.	25.0°	0.18	5.4°	0.26	-103.3	0.19

3.4.2 Spatial variability of detrended precipitation fields

On the smallest scales a strong difference is visible in variograms of detrended ~~filtered and detrended partially filtered~~ entirely-filtered and detrended partly-filtered radar precipitation, with weaker variability for ~~filtered data (Figure~~ entirely-filtered data (Fig. 6). ~~Smallest scale~~ Smallest-scale structures in the radar data are ~~very~~ likely an indicator of residual noise in the ~~partially filtered~~ partly-filtered radar data (Sect. 2.3). However, it could also imply micro-scale precipitation features. This stresses the challenge of processing ~~high resolution~~ high-resolution radar data (Sect. 2.3) to get a reasonable radar precipitation field. In any case the ~~filtered radar precipitation estimations~~ entirely-filtered radar precipitation estimates may be regarded as clean concerning residual clutter and will therefore be used for all subsequent analysis.

Variograms of ~~filtered~~ entirely-filtered and detrended radar precipitation show a steep increase of variability on the smallest scales, while the increase in variability gets weaker for larger scales (less steep slope in the variograms). Small-scale patterns are likely driven by small-scale precipitation cells induced by local cloud dynamics and microphysics. Such small-scale structures are repeated on intermediate scales and lead to a weaker increase in variability, as less new spatial features are added. At larger scales variability reaches the total variability of the detrended data.

Compared to radar precipitation WRF precipitation at 2830 m asl shows a lower variability and a flatter increase in variability at small scales giving evidence for a smoother precipitation distribution at the smallest scales compared to radar precipitation patterns. The lack of small-scale patterns clearly shows that the radar sees more variability at the smallest scales, while WRF likely misses the ~~smallest scale~~ smallest-scale processes. Variability of radar and WRF precipitation at 2830 m asl at large scales (> 5 km), especially on 4 February 2016, ~~is similar~~show less systematic differences than at small scales. This indicates that, with respect to total variability, patterns at these scales are well represented. Total ground precipitation shows a higher variability compared to precipitation at 2830 m asl (except for 4 February 2016), which is an indication that near-surface processes are active in the model.

Variograms of precipitation in the local domain (300 m resolution, ~~Figure~~ Fig. 1) look similar to variograms of the regional domain (450 m reoslution), but reach domain-wide variability at about 5 km lag distance (Supplementary Information ~~S1~~S2), while on the regional scale the domain-wide variability is reached at a distance of about 15–20 km (~~Figure~~ Fig. 6).

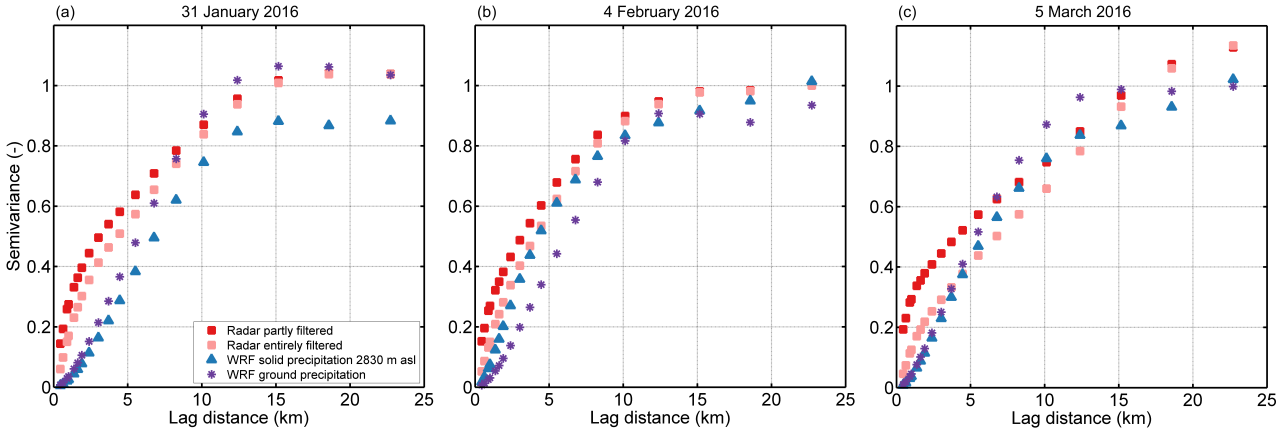

Figure 6. ~~Normalized variograms~~ Variograms of detrended snow precipitation normalized by the domain-wide variance of precipitation for the precipitation events on a) 31 January 2016, b) 4 February 2016 and c) 5 March 2016 for the regional domain (~~Figure~~ Fig. 1). Variograms are given for ~~partly filtered~~ partly-filtered (red) and ~~filtered~~ entirely-filtered (orange) radar snow precipitation, WRF snow precipitation at 2830 m above sea level (m asl, blue) and WRF total ground precipitation (violet). WRF precipitation is from simulations with weak terrain smoothing (Sect. 2.1). All precipitation fields are masked.

Furthermore, the difference between radar and WRF precipitation variability at small scales is larger ~~at~~ on the local domain compared to the regional domain. ~~This further shows that the model does not properly reproduce small-scale precipitation and deposition patterns, i.e. the radar sees more variability at the smallest scales~~ This and a systematic underestimation of precipitation variability at scales < 5 km (on the regional domain) compared to precipitation variability in radar estimates indicate that mountain ridge-scale precipitation processes are under-represented in the model.

3.4.3 Scale breaks and dominating processes

Scale breaks were previously found to be connected to changes in dominant processes (e.g. Deems et al., 2006). ~~To include~~ Here, we present a scale analysis including variability due to large-scale ~~processes~~precipitation processes. Therefore, we present variograms of non-detrended precipitation fields, being aware that a certain portion of the ~~small and intermediate scale~~ small- and intermediate-scale precipitation variability may become hidden. As precipitation patterns are known to be driven by topography and wind, we present variograms of topography together with the variograms of precipitation.

Variograms of topography clearly reveal two scale breaks (~~Figure~~ Fig. 7). The first scale break is between 1 and 2.5 km depending on the resolution, the second scale break is at 5 km and 6 km for real topography and weakly smoothed WRF topography, respectively. For topography the two scale breaks are separating the mountain-slope scale ($<\sim$ 1–2 km), mountain-ridge-to-valley scale (between $\sim$ 1–2 km and $\sim$ 5 km) and the scale of repeated mountain ridges and valleys ($>$ ~~5km~~5 km).

For consistency reasons, all variograms in ~~Figure~~ Fig. 7 are presented with two scale breaks. ~~Even though for precipitation some scale breaks are arbitrary, as the data do not reveal a clear scale break, the scale~~ Scale breaks for all events and both

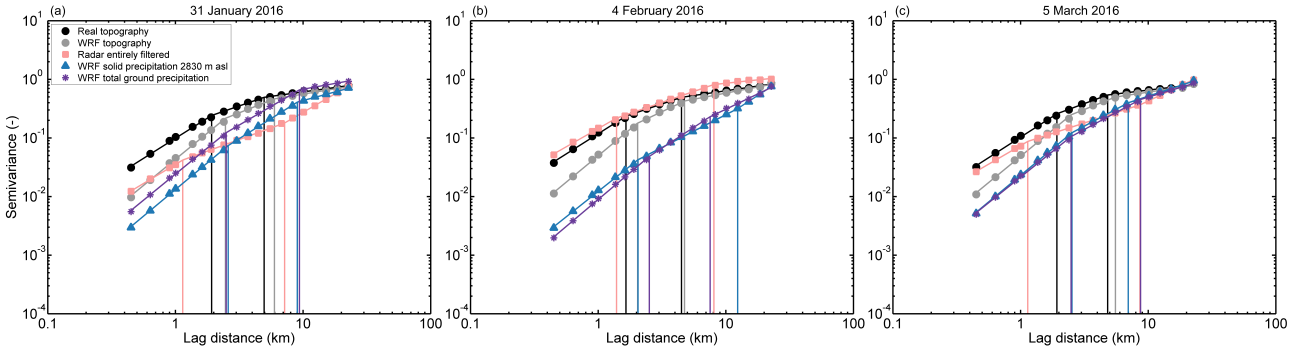

Figure 7. Normalized variograms of the snow precipitation events on a) 31 January 2016, b) 4 February 2016 and c) 5 March 2016 for the regional domain (~~Figure~~ Fig. 1). Variograms are given for ~~filtered~~ entirely-filtered radar snow precipitation (orange), WRF snow precipitation at 2830 m above sea level (m asl, blue) and WRF total ground precipitation (violet). Additionally, variograms are given for real topography (based on dhm25 © 2018 swisstopo (5740 000 000), black) and WRF topography (gray). WRF topography and precipitation are from simulations with weak terrain smoothing (Sect. 2.1). All precipitation fields are masked.

resolutions are basically grouped in two areas ($\sim$ 1–2.5 km and 5–10 km for 450 m resolution, ~~Figure~~ Fig. 7 and $\sim$ 800 m–1.2 km and 2.5–5 km for 300 m resolution, Supplementary Information ~~S1). Even though~~ S2), even though for precipitation some scale breaks are arbitrary. Albeit scale breaks of precipitation do not exactly match scale breaks of topography, breaks at similar scales as well as similar slopes of topography and precipitation at small scales support the interpretation of topography dependent precipitation patterns. On the smallest scales ($<$ 1–2 km) the slopes of precipitation variograms are similar to the slopes of the variograms of corresponding topography~~on these scales~~. This is an indication that precipitation patterns on mountain-slope scales may be terrain-driven. ~~The most likely reason for this is an elevation gradient in precipitation. Additional processes acting on~~ Processes acting at these scales could be small-scale cloud-dynamical processes such as the seeder-feeder mechanism (Bergeron, 1965; Purdy et al., 2005) or preferential deposition (Lehning et al., 2008). The latter is, however, for most mountain ridges unlikely to be seen in precipitation fields at 2830 m asl as it happens ~~very~~ close to the ground. ~~On~~ For the precipitation event on 5 March 2016, on scales $>$ 5–7 km ~~,~~ (i.e. for the scales above the second scale break~~, for the precipitation event on 5 March 2016~~) the slopes of the normalized variograms of radar and WRF precipitation at radar elevation are similar. Large-scale gradients at these scales are most likely driven by large-scale orographic precipitation enhancement (e.g. Stoelinga et al., 2013). Good agreement of the slopes in normalized variograms between radar and WRF precipitation is an indicator that the model has the potential to properly ~~represents~~ represent the strength of the large-scale gradient with respect to the overall variability, i.e. large-scale orographic precipitation enhancement. Disagreement of variograms of precipitation and topography ~~on~~ at these scales further support the hypothesis that ~~largest scale~~ largest-scale precipitation is mainly determined by ~~orographic~~ large-scale orographic precipitation enhancement, which introduces an increase in variability of precipitation at large scales, while large-scale topography reveals a repeated pattern of valleys and peaks (i.e. constant variability). Overall, this analysis supports the hypothesis in Sect. 3.2 that precipitation patterns in the regional domain are topography driven.

3.4.4 2-dimensional variability patterns

~~The~~ Finally, the combined influence of topography and the general wind direction on snow precipitation patterns in the ~~radar~~ regional domain is assessed by spatial 2D-autocorrelation maps (~~Figure~~ Fig. 8). Like variograms, autocorrelation is dependent on ~~large scale~~ large-scale trends. The general direction of 2D-autocorrelation patterns is the same for detrended (~~Figure~~ Fig. 8) and non-detrended (not shown) precipitation patterns. However, autocorrelation patterns of detrended precipitation fields show much shorter decorrelation lengths. This is due to the spatial coherence introduced by large-scale trends in precipitation. To avoid biased autocorrelation data, only 2D-autocorrelation maps of detrended precipitation fields are shown. However, we keep in mind that large-scale trends are present.

Autocorrelation maps of topography (~~Figures~~ Fig. 8a and Fig. 8e) represent a north-west to south-east oriented pattern which is, although weaker, repeated in south-west to north-east and west to east direction. For snow precipitation events with dominating north-westerly to northerly advection, the main axis of the snow precipitation 2D-autocorrelation pattern is oriented in a north-west to ~~south-easterly~~ south-east direction and therefore in alignment with both topography and the main wind direction (~~Figures~~ Fig. 8b-c and Fig. 8f-g). Patterns of WRF precipitation at 2830 m asl are rotated toward a north-south direction on 4 February 2016. For dominating southerly advection the 2D-autocorrelation map of radar precipitation shows a more homogeneous pattern compared to autocorrelation patterns for northern to north-western advection but a weak south-west to north-east orientation of ~~larger scale patterns (Figures~~ larger-scale patterns (Fig. 8d). For the WRF simulations a strong south-west to north-east orientation is present in the autocorrelation map ~~(Figure~~ for the precipitation event on 5 March 2016 (Fig. 8h). Even though isotropic variograms reveal good agreement in domain-wide variability, 2D-autocorrelation maps show that this may not necessarily go along with good agreement of the orientation of patterns. Best agreement in the orientation of patterns is found for 31 January 2016. For the three events, 2D-autocorrelation maps of detrended precipitation reveal a smoother distribution of precipitation on the smallest scales in the model compared to radar data, due to less small-scale structures in the model. On the other hand, a strong decrease in autocorrelation in east-west direction is visible for 5 March 2016. This shows that WRF simulations have a stronger ~~dependence~~ dependency on both wind direction and topography and tend to generate strong precipitation bands in the main wind direction, confirming the overly ~~idealistic~~ simplistic behavior of the model.

For ground precipitation 2D-autocorrelation patterns tend to be repeated in south-west to north-east and west to east direction as seen for topography (~~Figures~~ Figs. 8j-g). This stresses the hypothesis that the influence of topographic features on WRF ground precipitation is stronger than at radar elevation and gives evidence that these results are likely produced by near-surface topographically driven pre-depositional processes such as e.g. preferential deposition or the seeder-feeder mechanism in the model. While a topography dependency was already found in isotropic variograms, this 2D-autocorrelation analysis reveals that the wind direction additionally strongly impacts the snow precipitation distribution.

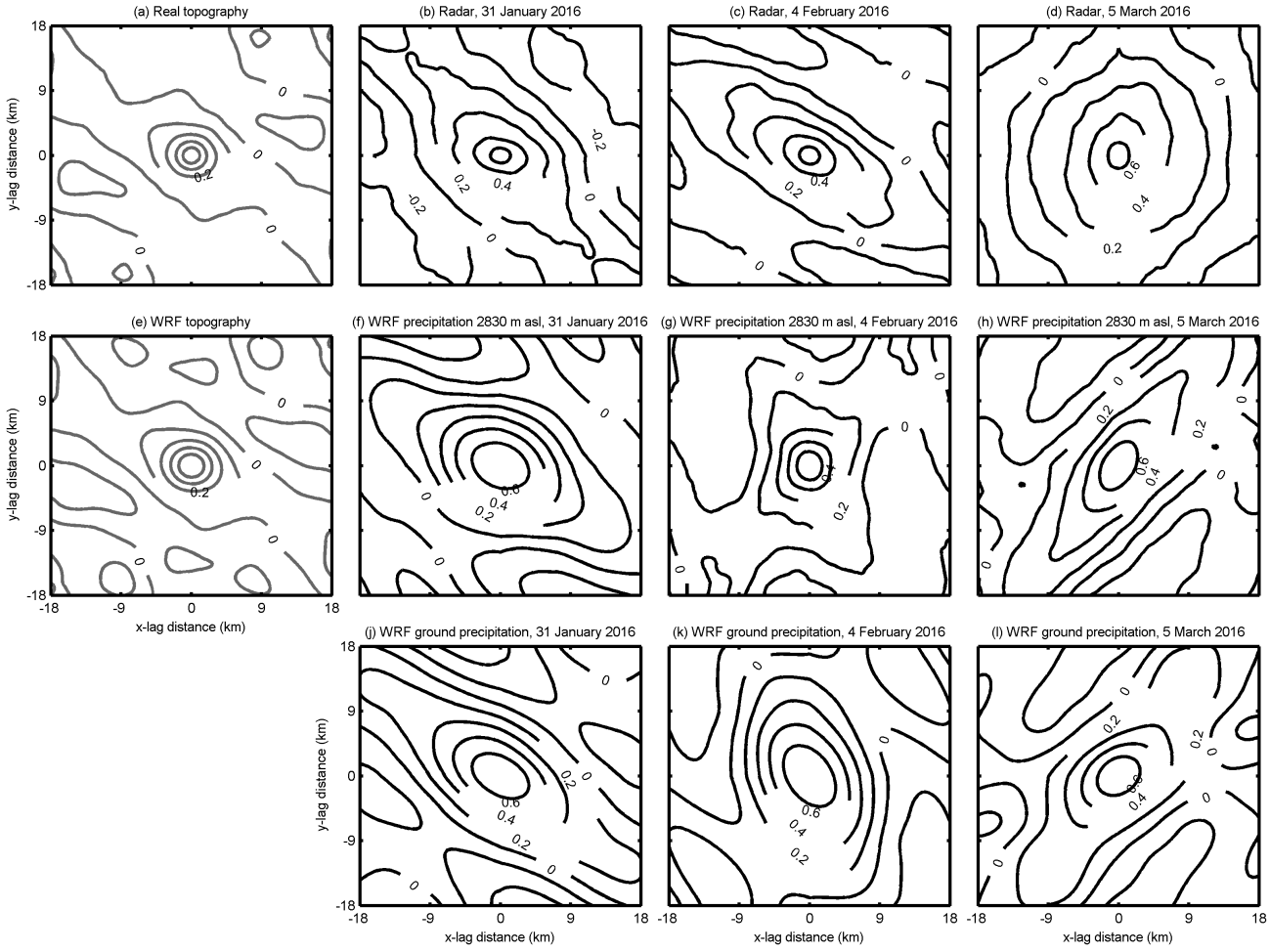

Figure 8. Spatial 2D-autocorrelation maps for the regional domain (450 m resolution) of detrended a) real topography (based on dhm25 © 2018 swisstopo (5740 000 000)), b)-d) entirely-filtered radar snow precipitation, e) WRF topography, f)-h) WRF snow precipitation at 2830 m above sea level (m asl) and j-l) WRF total ground precipitation. Autocorrelation maps of snow precipitation are for the three snow precipitation events on 31 January 2016, 4 February 2016 and 5 March 2016. WRF topography and precipitation are from simulations with weak terrain smoothing (Sect. 2.1). Radar precipitation and WRF precipitation at 2830 m asl are masked (as shown in ~~Figure~~ Fig. 4).

3.5 Dependence of spatial variability on model resolution and smoothing

Geostatistical ~~analysis show~~ analyses presented in this study demonstrate that precipitation on the regional scale (> ~~5km~~5 km) is reasonably represented in the WRF model, while small-scale ~~variability drops for model simulations at a resolution~~ precipitation variability is systematically underestimated in the model simulations with a horizontal grid spacing of 450 m

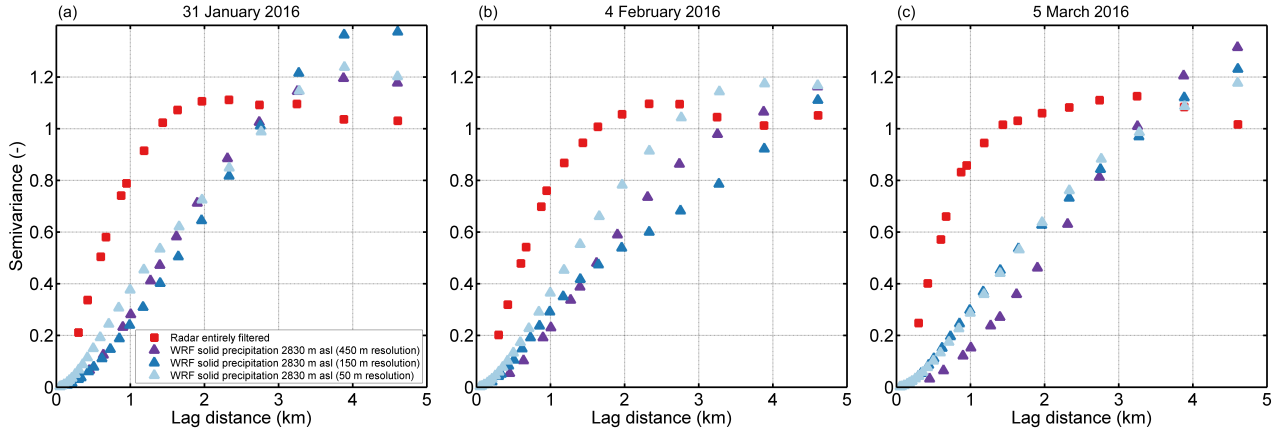

Figure 9. ~~Normalized variograms~~ Variograms of detrended snow precipitation normalized by the domain-wide variance of precipitation for the precipitation events on a) 31 January 2016, b) 4 February 2016 and c) 5 March 2016 for domain Dischma (~~Figure~~ Fig. 1). Variograms are given for ~~filtered~~ entirely-filtered radar snow precipitation (red), and WRF snow precipitation at 2830 m above sea level (m asl) with 450 m (violet), 150 m (blue) and 50 m (light blue) resolution. WRF snow precipitation is from simulations with weak terrain smoothing (Sect. 2.1). Radar precipitation is masked.

(Sect. 3.4). Variograms up to a maximum lag distance of 5 km on domain Dischma (~~Figure~~ Fig. 1) reveal an increase of variability for increasing model resolution (~~Figure~~ Fig. 9). However, simulated variability stays far below the variability of ~~filtered~~ entirely-filtered radar precipitation. Depending on the event an increase in variability is present for 150 m and 50 m resolution. ~~Smallest scale~~ This indicates that smallest-scale precipitation dynamics are still not fully resolved at 50 m resolution. A comparison of variograms for simulations with strongly smoothed terrain compared to simulations with weaker terrain smoothing (Sect. 2.1) reveal that a stronger terrain smoothing may result in less explained variability in normalized variograms (not shown). Even though this signal is not consistent for all events, we can show that a better representation of topography due to higher resolution and less smoothing has the potential to increase the explained variability of precipitation patterns. An increase in variability ~~is mainly present at the smallest scales , indicating~~ at small scales (< 5 km), indicates that more small-scale patterns are ~~represented~~ resolved at higher resolutions (50 m horizontal grid spacing) in the model. Our simulations are currently limited to the presented resolutions and strong terrain smoothing due to model instabilities. However, based on the presented results, once available, the immersed boundary ~~model~~ method version of WRF (e.g. Lundquist et al., 2010, 2012; Arthur et al., 2016; Ma and Liu, 2017), will likely be a good tool to allow for steeper slopes in the simulation and going toward higher resolution LES simulations to resolve further small-scale wind fields, which drive the precipitation structures.

4 Conclusions and Outlook

The implementation of COSMO–WRF is a ~~step toward~~ further step in performing very-high resolution precipitation simulations in complex alpine terrain to address the question of the relative importance of cloud-dynamics and ~~pure~~ particle-flow interactions on a mountain-ridge scale. ~~We~~ In this validation study, we show that COSMO–WRF is able to reasonably simulate atmospheric conditions, but tends to overestimate near-surface wind speeds, which may be due to many reasons from an overestimation of speed-up effects to an underrepresentation of ~~topographic~~ small terrain features. Relative humidity patterns are highly variable and may be a sign ~~of overestimated~~ that subsidence and lifting ~~in the model~~produce too strong effects in the (partially parameterized) cloud dynamics, given the good representation of topography at larger scales.

Regional and local scale precipitation patterns in the COSMO–WRF simulations are in partially good agreement with MeteoSwiss operational radar measurements and automatic weather stations. For the three events analyzed here, precipitation ~~estimations~~ estimates from WRF simulations are higher compared to precipitation ~~estimation~~ estimates from radar measurements. A general overestimation of precipitation produced by WRF is consistent with an overestimation of subsidence and lifting. Overestimation of precipitation in WRF simulations has ~~, however,~~ been documented previously for snow precipitation over complex terrain (e.g. Silverman et al., 2013), likely due to the high model resolution and therefore more complex topography and higher mountain peaks compared to common high resolution simulations.

An autocorrelation and scale analysis of radar and WRF snow precipitation reveals a good agreement of precipitation patterns on regional scales (> 5 km), which are topography and wind driven. These large-scale patterns are in good agreement with the theory of large-scale orographic enhancement (e.g. Stoelinga et al., 2013). Disagreement in precipitation patterns i.e. a downwind shift of snow ~~accumulation~~ precipitation in the WRF simulations compared to radar precipitation estimates is likely due to lifting condensation being too weak in ~~the north-western part of the domain~~areas, where topography is lower and strong smoothing leads to an underrepresentation of topography. On the other hand, over peaks, which are high and steep enough in the model to allow for lifting condensation, the effect of orographic precipitation enhancement tends to be overestimated. An increase of this overestimation of precipitation over high elevations for higher resolution simulations as well as for weaker terrain smoothing supports this hypothesis. Smallest-scale patterns in the radar measurements are likely dominated by noise, which is removed by the application of a median filter. Given these uncertainties the radar data cannot be considered as the absolute reference. ~~When observing with a critical eye~~In case of critical data analysis, an estimation of ~~high resolution~~ high-resolution radar precipitation is, however, ~~very~~ useful to improve the understanding of precipitation processes in complex terrain and to validate and improve model simulations. On a local to mountain-valley scale WRF simulations ~~show much less~~ systematically show a lower variability of precipitation compared to radar ~~estimations~~estimates. This indicates that the model is not able to represent the full spectrum of small-scale precipitation patterns, which are present in the radar measurements~~as most likely the representation~~ . One potential reason for the lack of precipitation variability is the simplification of cloud dynamics and microphysics in the model~~is too idealistic, due to the given resolution~~, typically used to model regional-scale precipitation fields. Additionally, we could show that the underrepresentation of topography may have a strong influence on the formation of local low-level clouds, which are important for orographic precipitation enhancement. This is supported by

the fact that precipitation patterns in the model show a stronger ~~dependence~~ dependency on topography and wind direction than precipitation patterns in the radar estimates. However, an increase in precipitation variability at scales < 5 km is visible for higher resolution WRF simulations. Furthermore, for simulations with steeper terrain an increase in variability for all resolutions is found. This shows that especially for small-scale variability a better representation of the complex terrain is essential to reproduce precipitation variability. Although the model cannot represent the full variability measured by the radar at small scales, an increase in precipitation between 2830 m asl and the ground is an indication that the model captures a certain portion of near-surface processes.

To specifically address processes such as the seeder-feeder mechanism or preferential deposition an analysis of hydrometeors and precipitation distributions in vertical profiles across mountain ridges is needed. To connect pre-depositional processes with post-depositional processes even higher resolution WRF simulations would be ~~needed~~required. This might be achieved by employing the immersed-boundary method version setup of WRF. A parameterization of post-depositional processes in WRF or using WRF simulations as a boundary condition for simulations with the Alpine surface processes model Alpine3D (Lehning et al., 2008), would then allow validation of modeled snow accumulation patterns compared to measured snow accumulation patterns. Furthermore, simulations of precipitation patterns in complex terrain need to be analyzed with higher temporal resolution (e.g. on the order of minutes), as contributing processes show high temporal variability. Future work will include addressing the temporal variability of precipitation patterns using radar observations, along with an analysis of precipitation growth with respect to topography and wind direction.

Code and data availability. A COSMO–WRF documentation is published as Gerber and Sharma (2018). Data can be made available upon request.

Appendix A: Morrison microphysics in WRF

The Morrison microphysics scheme includes prognostic equations of number concentration and mass mixing ratio of 5 precipitation species (rain, snow, ice, graupel and cloud droplets). The parametrization of rain, snow, ice and cloud droplets is based on Morrison et al. (2005). The implementation of graupel follows Reisner et al. (1998), except for minimum mixing ratios, which are required to produce graupel from the collision of rain and snow, snow and cloud water, and rain and cloud ice, which are based on Rutledge and Hobbs (1984).

The kinetic equations include advection, sedimentation and turbulent diffusion as well as source and sink terms of ice nucleation and droplet activation, condensation and deposition, coalescence and diffusional growth, collection, melting and freezeing as well as ice multiplication (Morrison et al., 2005). For graupel deposition, collection, collision, accretion, freezing and melting processes are parameterized (Reisner et al., 1998).

Size distribution functions are gamma functions:

$$N(D) = N_0 D^{\mu} e^{-\lambda D}, \tag{A1}$$

where D is the particle diameter, μ is the shape parameter of the distribution function, which is $\mu = 0$ for rain, snow, ice and graupel, resulting in an exponential function for N(D). λ and N_0 are the slope and intercept, respectively, of the size distribution, evaluated by the predicted number concentration N and mass mixing ratio q:

$$\lambda = [\frac{cN\Gamma(\mu + d + 1)}{q\Gamma(\mu + 1)}]^{1/d} \tag{A2}$$

and

$$N_0 = \frac{N\lambda^{\mu+1}}{\Gamma(\mu + 1)}, \tag{A3}$$

where Γ is the gamma-function. c and d are the parameters of the power-law function $m = cD^d$ indicating the mass-diameter relationship. Terminal fallspeeds are as well assumed to have a power-law form of $v(D) = \frac{\rho_{sur}}{\rho} aD^b$, with individual parameters a and b for the different species. ρ is the air density and ρ_{sur} the air density at sea level. For simplification all species are assumed to be spheres. Additionally, the particles do not have any particle inertia.

Author contributions. FG and NB performed the analysis, which was supported by fruitful discussions with ML, RM, AB and UG. FG, VS, MD, RM and ML developed the COMSO-WRF coupling and simulation setup, which were run by FG. NB and MG processed the radar data. FG, ML, RM, NB and AB contributed to the design of the concept. FG and NB with contributions of all authors prepared the manuscript.

Acknowledgements. The work is funded by the Swiss National Science Foundation (Project: Snow-atmosphere interactions driving snow accumulation and ablation in an alpine catchment: The Dischma Experiment; SNF-grant: 200021_150146 and project: The sensitivity of very small glaciers to micrometeorology; SNF-grant: P300P2_164644). Topographic data are reproduced by permission of swisstopo (JA100118). For advice to setup WRF simulations we thank the WRF-help. For supporting our project with computational time many thanks go the the Swiss National Supercomputing Center (CSCS) and their support for technical advice. Additionally, we thank the Swiss Federal Office of Meteorology and Climatology (MeteoSwiss) for providing access to radar data, COSMO–2 ~~reanalysis~~ analysis and the regridding tool fieldextra. For advice related to COSMO–2 thanks go to Guy de Morsier from MeteoSwiss. Further thanks go to Amalia Iriza and Rodica Dumitrache from MeteoRomania for advice concerning the COSMO–WRF coupling. Additional thanks go to Louis Quéno and Benoit Gherardi for their work on pre-preprocessing steps and data processing to setup WRF simulations. Additionally, we thank Heini Wernli and the two anonymous reviewers for their questions, comments and recommendations, which helped to improve the paper.

References

Arnold, D., Schicker, I., and Seibert, P.: High-Resolution Atmospheric Modelling in Complex Terrain for Future Climate Simulations(HiRmod), Report 2010, Tech. rep., Institute of Meteorology (BOKU-Met), University of Natural Resources and Life Sciences, Vienna, Austria, http://www.wau.boku.ac.at/met/envmet/hirmod.html, 2010.

Arthur, R., Lundquist, K. A., Mirocha, J. D., Hoch, S. W., and Chow, F. K.: High-resolution simulations of downslope flows over complex terrain using WRF-IBM, 17th Conference on Mountain Meteorology, Armerican Meteorological Society, Paper 7.6, 18 pages, 2016.

Beljaars, A. C. M.: The parameterization of surface fluxes in large-scale models under free convection, Quarterly Journal of the Royal Meteorological Society, 121, 255 – 270, https://doi.org/10.1002/qj.49712152203, 1994.

Bergeron, T.: On the low-level redistribution of atmospheric water caused by orography., Suppl. Proc. Int. Conf. Cloud Phys., Tokyo, 96–100, 1965.

Besic, N., Figueras i Ventura, J., Grazioli, J., Gabella, M., Germann, U., and Berne, A.: Hydrometeor classification through statistical clustering of polarimetric radar measurements: a semi-supervised approach, Atmospheric Measurement Techniques, 9, 4425–4445, https://doi.org/10.5194/amt-9-4425-2016, 2016.

Caldwell, P., Chin, H., Bader, D., and Bala, G.: Evaluation of a WRF dynamical downscaling simulation over California, Climate Change, 95, 499–521, https://doi.org/10.1007/s10584-009-9583-5, 2009.

Choularton, T. W. and Perry, S. J.: A model of the orographic enhancement of snowfall by the seeder-feeder mechanism, Quarterly Journal of the Royal Meteorological Society, 112, 335–345, https://doi.org/10.1002/qj.49711247204, 1986.

Colle, B.: Sensitivity of orographic precipitation to changing ambient conditions and terrain geometries: An idealized modelling perspective, Journal of Atmospheric Sciences, 61, 588–606, https://doi.org/10.1175/1520-0469(2004)061<0588:SOOPTC>2.0CO;2, 2004.

Cooper, S. J., Wood, N. B., and L'Ecuyer, T. S.: A variational technique to estimate snowfall rate from coincident radar, snowflake, and fall-speed observations, Atmospheric Measurement Techniques, 10, 2557 — 2571, https://doi.org/10.5194/amt-10-2557-2017, 2017.

Dadic, R., Mott, R., Lehning, M., and Burlando, P.: Wind influence on snow depth distribution and accumulation over glaciers, Journal of Geophysical Research, 115, F01 012, https://doi.org/10.1029/2009JF001261, 2010.

Daniels, M. H., Lundquist, K. A., Mirocha, J. D., Wiersema, D. J., and Chow, F. K.: A New Vertical Grid Nesting Capability in the Weather Research and Forecasting (WRF) Model, Monthly Weather Review, 144, 3725 – 3747, https://doi.org/10.1175/MWR-D-16-0049.1, 2016.

Deems, J. S., Fassnacht, S. R., and Elder, K. J.: Fractal Distribution of Snow Depth from Lidar Data, Journal of Hydrometeorology, 7, 285 – 297, https://doi.org/10.1175/JHM487.1, 2006.

Deems, J. S., Fassnacht, S. R., and Elder, K. J.: Interannual Consistency in Fractal Snow Depth Patterns at Two Colorado Mountain Sites, Journal of Hydrometeorology, 9, 977 – 988, https://doi.org/10.1175/2008JHM901.1, 2008.

Dore, A. J., Choularton, T. W., Fowler, D., and Crossely, A.: Orographic enhancement of snowfall, Environ. Pollut., 75, 175–179, https://doi.org/10.1016/0269-7491(92)90037-B, 1992.

Dyer, A. J. and Hicks, B. B.: Flux-gradient relationships in the constant flux layer, Quarterly Journal of the Royal Meteorological Society, 96, 715– 721, https://doi.org/10.1002/qj.49709641012, 1970.

European Environmental Agency: CORINE Land Cover (CLC) 2006 raster data, Version 13, 2006.

Gabella, M., Speirs, P., Hamann, U., Germann, U., and Berne, A.: Measurement of Precipitation in the Alps Using Dual-Polarization C-Band Ground-Based Radars, the GPM Spaceborne Ku-Band Radar, and Rain Gauges, Remote Sensing, 9, https://doi.org/10.3390/rs9111147, 2017.

Gerber, F. and Sharma, V.: Running COMO-WRF on very high resolution over complex terrain, Laboratory of Cryospheric Sciences, École Polytechnique Fédérale de Lausanne, Lausanne, Switzerland, https://doi.org/10.16904/envidat.35, 2018.

Gerber, F., Lehning, M., Hoch, S. W., and Mott, R.: A close-ridge small-scale atmospheric flow field and its influence on snow accumulation, Journal of Geophysical Research – Atmospheres, 122, 7737 – 7754, https://doi.org/10.1002/2016JD026258, 2017.

Germann, U., Galli, G., Boscacci, M., and Bolliger, M.: Radar precipitation measurement in a mountainous region, Quarterly Journal of the Royal Meteorological Society, 132, 1669–1692, https://doi.org/10.1256/qj.05.190, 2006.

Germann, U., Boscacci, M., Gabella, M., and Sartori, M.: Peak performance: Radar design for prediction in the Swiss Alps, Meteorological Technology International, pp. 42–45, 2015.

Gómez-Navarro, J. J., Raible, C. C., and Dierer, S.: Sensitivity of the WRF model to PBL parametrisations and nesting techniques: evaluation of wind storms over complex terrain, Geoscientific Model Development, 8, 3349 – 3363, https://doi.org/10.5194/gmd-8-3349-2015, 2015.

Grünewald, T., Schirmer, M., Mott, R., and Lehning, M.: Spatial and temporal variability of snow depth and ablation rates in a small mountain catchment, The Cryosphere, 4, 215–225, https://doi.org/10.5194/tc-4-215-2010, http://www.the-cryosphere.net/4/215/2010/, 2010.

Grünewald, T., S., D., Cattin, R., Steiner, P., Steinkogler, W., Fundel, F., and Lehning, M.: Mapping frequencies of icing on structures in Switzerland, Journal of Engineering and Industrial Aerodynamics, 107–108, 76–82, https://doi.org/10.1016/j.jweia.2012.03.022, 2012.

Hong, S.-Y., Noh, Y., and Dudhia, J.: A New Diffusion Package with an Explicit Treatment of Entrainment Processes, Monthly Weather Review, 134, 2318 – 2341, https://doi.org/10.1175/MWR3199.1, 2006.

Houze, Jr., R. A.: Orographic effects on precipitating clouds, Reviews of Geophysics, 50, RG1001, https://doi.org/10.1029/2011RG000365, 2012.

Huwald, H., Higgins, C. W., Boldi, M.-O., Bou-Zeid, E., Lehning, M., and Parlange, M. B.: Albedo effect on radiative errors in air temperature measurements, Water Resources Research, 45, W08 431, https://doi.org/10.1029/2008WR007600, 2009.

Jiménez, P. A. and Dudhia, J.: Improving the Representation of Resolved and Unresolved Topographic Effects on Surface Wind in the WRF Model, Journal of Applied Meteorology and Climatology, 51, 300 – 316, https://doi.org/10.1175/JAMC-D-11-084.1, 2012.

Lehning, M. and Fierz, C.: Assessment of snow transport in avalanche terrain, Cold Regions Science and Technology, 51, 240–252, https://doi.org/10.1016/j.coldregions.2007.05.012, 2008.

Lehning, M., Löwe, H., Ryser, M., and Raderschall, N.: Inhomogeneous precipitation distribution and snow transport in steep terrain, Water Resources Research, 44, W07 404, https://doi.org/10.1029/2007WR006545, http://dx.doi.org/10.1029/2007WR006545, 2008.

Leung, L. R. and Qian, Y.: The sensitivity of precipitation and snowpack simulations to model resolution via nesting in regions of complex terrain, Journal of Hydrometeorology, 4, 1025 – 1043, https://doi.org/10.1175/1525-7541(2003)004<1025:TSOPAS>2.0.CO;2, 2003.

Liu, C., Ikeda, K., Thompson, G., Rasmussen, R., and Dudhia, J.: High-Resolution Simulations of Wintertime Precipitation in the Colorado Headwaters Region: Sensitivity to Physics Parameterizations, Monthly Weather Review, 139, 3533 – 3553, https://doi.org/10.1175/MWR-D-11-00009.1, 2011.

Lundquist, K. A., Chow, F. K., and Lundquist, J. K.: An immersed boundary method for the Weather Research and Forecasting model, Monthly Weather Review, 138, 796–817, https://doi.org/10.1175/2009MWR2990.1, 2010.

Lundquist, K. A., Chow, F. K., and Lundquist, J. K.: An Immersed Boundary Method Enabling Large-Eddy Simulations of Flow over Complex Terrain in the WRF Model, Monthly Weather Review, 140, 3936–3955, https://doi.org/10.1175/MWR-D-11-00311.1, 2012.

Ma, Y. and Liu, H.: Large-Eddy Simulations of Atmospheric Flows Over Complex Terrain Using the Immersed-Boundary Method in the Weather Research and Forecasting Model, Boundary-Layer Meteorology, 165, 421 – 445, https://doi.org/10.1007/s10546-017-0283-9, 2017.

Mass, C., Ovens, D., Westrick, K., and Colle, B. A.: Does increasing horizontal resolution produce more skillful forecasts?, Bulletin of the American Meteorological Society, 83, 407 – 430, https://doi.org/10.1175/1520-0477(2002)083<0407:DIHRPM>2.3.CO;2, 2002.

METI/NASA: 2009, ASTER Global Digital Elevation Model V002, NASA EOSDIS Land Processes DAAC, USGS Earth Resources Observation and Science (EROS) Center, Sioux Falls, South Dakota (https://lpdaac.usgs.gov), accessed 01 24, 2018, at http://dx.doi.org/10.5067/ASTER/ASTGTM.002. Aster GDEM is a product of NASA and METI., 2009.

Mirocha, J., Kosović, B., and Kirkil, G.: Resolved Turbulence Characteristics in Large-Eddy Simulations Nested within Mesoscale Simulations Using the Weather Research and Forecasting Model, Monthly Weather Review, 142, 806–831, https://doi.org/10.1175/MWR-D-13-00064.1, 2014.

Mirocha, J. D., Lundquist, J. K., and Kosović, B.: Implementation of a Nonlinear Subfilter Turbulence Stress Model for Large-Eddy Simulation in the Advanced Research WRF Model, Monthly Weather Review, 138, 4212–4228, https://doi.org/10.1175/2010MWR3286.1, 2010.

Morrison, H., Curry, J. A., and Khvorostyanov, V. I.: A New Double-Moment Microphysics Parameterization for Application in Cloud and Climate Models. Part I: Description, Journal of Atmospheric Sciences, 62, 1665 – 1677, https://doi.org/10.1175/JAS3446.1, 2005.

Morrison, H., Thompson, G., and Tatarskii, V.: Impact of Cloud Microphysics on the Development of Trailing Stratiform Precipitation in a Simulated Squall Line: Comparison of One- and Two-Moment Schemes, Monthly Weather Review, 137, 991–1007, https://doi.org/10.1175/2008MWR2556.1, 2009.

Mott, R. and Lehning, M.: Meteorological Modeling of Very High-Resolution Wind Fields and Snow Deposition for Mountains, Journal of Hydrometeorology, 11, 934–949, https://doi.org/10.1175/2010JHM1216.1, 2010.

Mott, R., Schirmer, M., Bavay, M., Grünewald, T., and Lehning, M.: Understanding snow-transport processes shaping the mountain snow-cover, The Cryosphere, 4, 545–559, https://doi.org/10.5194/tc-4-545-2010, 2010.

Mott, R., Schirmer, M., and Lehning, M.: Scaling properties of wind and snow depth distribution in an Alpine catchment, Journal of Geophysical Research, 116, D06 106, https://doi.org/10.1029/2010JD014886, 2011.

Mott, R., Scipión, D., Schneebeli, M., Dawes, N., Berne, A., and Lehning, M.: Orographic effects on snow deposition patterns in mountainous terrain, Journal of Geophysical Research – Atmospheres, 119, 1419–1439, https://doi.org/10.1002/2013JD019880, http://dx.doi.org/10.1002/2013JD019880, 2014.

Mott, R., Daniels, M., and Lehning, M.: Atmospheric Flow Development and Associated Changes in Turbulent Sensible Heat Flux over Patchy Mountain Snow Cover, Journal of Hydrometeorology, 16, 1315–1340, https://doi.org/10.1175/JHM-D-14-0036.1, 2015.

Mott, R., Schlögl, S., Dirks, L., and Lehning, M.: Impact of Extreme Land Surface Heterogeneity on Micrometeorology over Spring Snow Cover, Journal of Hydrometeorology, 18, 2705–2722, https://doi.org/10.1175/JHM-D-17-0074.1, 2017.

Muñoz Esparza, D., Lundquist, J. K., Sauer, J. A., Kosovic, B., and Linn, R. R.: Coupled mesoscale-LES modeling of a diurnal cycle during the CWEX-13 field campaign: From weather to boundary-layer eddies, Journal of Advances in Modeling Earth Systems, 9, 1572 – 1594, https://doi.org/10.1002/2017MS000960, 2017.

Niu, G.-Y., Yang, Z.-L., Mitchell, K. E., Chen, F., Ek, M. B., Barlage, M., Kumar, A., Manning, K., Niyogi, D., Rosero, E., Tewari, M., and Xia, Y.: The community Noah land surface model with multiparameterization options (Noah-MP): 1. Model description and evaluation with local-scale measurements, Journal of Geophysical Research, 116, D12 109, https://doi.org/10.1029/2010JD015139, 2011.

Obukhov, A. M.: Turbulence in an atmosphere with a non-uniform temperature, Boundary-Layer Meteorology, 2, 7 – 29, 1971.

Panziera, L., James, C. N., and Germann, U.: Mesoscale organization and structure of orographic precipitation producing flash floods in the Lago Maggiore region, Quarterly Journal of the Royal Meteorological Society, 141, 224–248, https://doi.org/10.1002/qj.2351, 2015.

Paulson, C. A.: The mathematical representation of wind speed and temperature profiles in the unstable atmospheric surface layer, Journal of Applied Meteorology, 9, 857 – 861, https://doi.org/10.1175/1520-0450(1970)009<0857:TMROWS>2.0.CO;2, 1970.

Pineda, N., Jorba, O., Jorge, J., and Baldasano, J. M.: Using NOAA AVHRR and SPOT VGT data to estimate surface parameters: application to a mesoscale meteorological model, International Journal of Remote Sensing, 25, 129 – 143, https://doi.org/10.1080/0143116031000115201, 2004.

Pohl, B.: Testing WRF capability in simulating the atmospheric water cycle over Equatorial East Africa, Climate Dynamics, 37, 1375–1379, https://doi.org/10.1007/s00382-011-1024-2, 2011.

Prokop, A.: Assessing the applicability of terrestrial laser scanning for spatial snow depth measurements, Cold Regions Science and Technology, 54, 155 – 163, https://doi.org/10.1016/j.coldregions.2008.07.002, 2008.

Purdy, J. C., Austin, G. L., W., S. A., and Cluckie, I. D.: Radar evidence of orographic enhancement due to the seeder feeder mechanism, Meteorological Applications, 12, 199 – 206, https://doi.org/10.1017/S1350482705001672, 2005.

Reisner, J., Rasmussen, R. M., and Bruintjes, R. T.: Explicit forecasting of supercooled liquid water in winter storms using the MM5 mesoscale model, Quarterly Journal of the Royal Meteorological Society, 124, 1071 – 1107, https://doi.org/10.1002/qj.49712454804, 1998.

Rutledge, S. A. and Hobbs, P. V.: The mesoscale and microscale structure of organization of clouds and precipitation in midlatitude cyclones. XII: A diagnostic modeling study of precipitation development in narrow cold-frontal rainbands, Journal of Atmospheric Sciences, 41, 2949 – 2972, https://doi.org/10.1175/1520-0469(1984)041<2949:TMAMSA>2.0.CO;2, 1984.

Saltikoff, E., Lopez, P., Taskinen, A., and Pulkkinen, S.: Comparison of quantitative snowfall estimates from weather radar, rain gauges and a numerical weather prediction model, Boreal environment research, 20, 667–678, 2015.

Schirmer, M. and Lehning, M.: Persistence in intra-annual snow depth distribution: 2. Fractal analysis of snow depth development, Water Resources Research, 47, W09 517, https://doi.org/10.1029/2010WR009429, 2011.

Schirmer, M., Wirz, V., Clifton, A., and Lehning, M.: Persistence in intra-annual snow depth distribution: 1. Measurements and topographic control, Water Resources Research, 47, W09 516, https://doi.org/10.1029/2010WR009426, 2011.

Schlögl, S., Lehning, M., and Mott, R.: Representation of horizontal transport processes in snowmelt modelling by applying a footprint approach, Frontiers in Earth Science, submitted.

Schmucki, E., Marty, C., Fierz, C., Weingartner, R., and Le: Impact of climate change in Switzerland on socioeconomic snow indices, Theoretical and Applied Climatology, 127, 875 – 889, https://doi.org/10.1007/s00704-015-1676-7, 2017.

Scipión, D. E., Mott, R., Lehning, M., Schneebeli, M., and Berne, A.: Seasonal small-scale spatial variability in alpine snowfall and snow accumulation, Water Resources Research, 49, 1446–1457, https://doi.org/10.1002/wrcr.20135, http://dx.doi.org/10.1002/wrcr.20135, 2013.

Silverman, N. L., Maneta, M. P., Chen, S.-H., and Harper, J. T.: Dynamically downscaled winter precipitation over complex terrain of the Central Rockies of Western Montana, USA, Water Resources Research, 49, 458 – 470, https://doi.org/10.1029/2012WR012874, 2013.

Skamarock, W. C., Klemp, J. B., Dudhia, J., Gill, D. O., Barker, D. M., Duda, M. G., Huang, X.-Y., Wang, W., and Powers, J. G.: A Description of the Advanced Research WRF Version 3, Tech. rep., Mesoscale and Microscale Meteorological Division, National Center for Atmospheric Research, Boulder, Colorado, USA, 2008.

Stoelinga, M. T., Stewart, R. E., Thompson, G., and Thériault, J. M.: Mountain Weather Research and Forecasting: Recent Progress and Current Challenges, chap. Microphysical Processes Within Winter Orographic Cloud and Precipitation Systems, pp. 345–408, Springer Netherlands, https://doi.org/10.1007/978-94-007-4098-3_7, http://dx.doi.org/10.1007/978-94-007-4098-3_7, 2013.

Talbot, C., Bou-Zeid, E., and Smith, J.: Nested Mesoscale Large-Eddy Simulations with WRF: Performance in Real Test Cases, Journal of Hydrometeorology, 13, 1421 – 1441, https://doi.org/10.1175/JHM-D-11-048.1, 2012.

Tedesche, M. E., Fassnacht, S. R., and Meiman, P. J.: Scales of snow depth variability in high elevation rangeland sagebush, 11, 469–481, https://doi.org/10.1007/s11707-017-0662-z, 2017.

Trujillo, E., Molotch, N. P., Goulden, M. L., Kelly, A. E., and Bales, R. C.: Elevation-dependent influence of snow accumulation on forest greening, Nature Geoscience, 5, 705–709, https://doi.org/10.1038/ngeo1571, 2012.

Vionnet, V., Martin, E., Masson, V., Lac, C., Naaim Bouvet, F., and Guyomarc'h, G.: High-resolution large eddy simulation of snow accumulation in alpine terrain, Journal of Geophysical Research – Atmospheres, 122, 11,005–11,021, https://doi.org/10.1002/2017JD026947, 2017.

Webb, E. K.: Profile relationships: The log-linear range, and extension to strong stability, Quarterly Journal of the Royal Meteorological Society, 96, 67 – 90, https://doi.org/10.1002/qj.49709640708, 1970.

Wyngaard, J. C.: Toward Numerical Modeling in the "Terra Incognita", Journal of Atmospheric Sciences, 61, 1816 – 1826, https://doi.org/10.1175/1520-0469(2004)061<1816:TNMITT>2.0.CO;2, 2004.

Yang, Z.-L., Niu, G.-Y., Mitchell, K. E., Chen, F., Ek, M. B., Barlage, M., Longuevergne, L., Manning, K., Niyogi, D., Tewari, M., and Xia, Y.: The community Noah land surface model with multiparameterization options (Noah-MP): 2. Evaluation over global river basins, Journal of Geophysical Research, 116, D12 110, https://doi.org/10.1029/2010JD015140, 2011.

Zängl, G.: The temperature dependence of small-scale orographic precipitation enhancement, Quarterly Journal of the Royal Meteorological Society, 134, 1167–1181, https://doi.org/10.1002/qj.267, 2008.

Zängl, G., Aulehner, D., Wastl, C., and Pfeiffer, A.: Small-scale precipitation variability in the Alps: Climatology in comparison with semi-idealized numerical simulations, Quarterly Journal of the Royal Meteorological Society, 134, 1865–1880, https://doi.org/10.1002/qj.311, 2008.

Zhang, D.-L. and Anthes, R. A.: A High-Resolution Model of the Planetary Boundary Layer – Sensitivity Tests and Comparisons with SESAME-79 Data, Journal of Applied Meteorology, 21, 1594 – 1609, https://doi.org/10.1175/1520-0450(1982)021<1594:AHRMOT>2.0.CO;2, 1982.

S1. Model levels

Table S.1 gives the first 21 model levels all four model domains (d01–d04).

Table S.1. First 21 model levels for all four model domains (d01–d04).

	Domains			
Level	d01	d02	d03	d04
	m	m	m	m
1	24.1	23.1	22.6	3.1
2	83.0	79.7	77.6	9.4
3	163.4	156.9	152.7	18.8
4	265.7	255.4	248.1	31.4
5	394.5	379.1	368.0	44.0
6	558.2	536.2	519.9	56.6
7	758.7	728.0	705.4	94.5
8	944.0	904.9	848.5	158.0
9	1098.5	1051.7	933.9	221.9
10	1255.8	1200.7	1020.1	286.2
11	1416.0	1352.0	1107.1	351.0
12	1657.3	1578.9	1237.5	416.2
13	1979.9	1881.7	1411.3	481.6
14	2305.8	2187.1	1585.9	547.8
15	2635.0	2495.1	1761.4	614.3
16	2967.6	2805.8	1937.8	681.2
17	3303.8	3119.3	2115.2	748.6
18	3643.7	3435.7	2293.7	811.9
19	3987.4	3755.2	2473.2	871.2
20	4335.0	4078.0	2653.9	930.8
21	4686.8	4404.4	2835.6	990.7

S2. Variability at the local domain

Figure S.1 show the domain-wide statistics of the local domain, for which data has a resolution of 300 m (Figure 1 in the main text). Variograms analogously to Figure 6 and Figure 7 in the main text are presented for the local domain. Trends removed from the data to produce the variograms in Figure S.2 are given in Table S.2. For Figure S.3 no trends are removed to retain the effect of large-scale precipitation processes. Thus, small as well as intermediate scale patterns may be hidden by the domain-wide trends.

Table S.2. Large-scale linear trends of entirely-filtered radar and WRF precipitation patterns on the local domain (Figure 1 in the main text). *Orientation* gives the direction of the slope and *Intensity* the strength of inclination. 0° would indicate a slope pointing toward the East. WRF snow precipitation is from simulations with weak terrain smoothing (Sect. 2.1 in the main text).

	31 January 2016		4 February 2016		5 March 2016	
	Orientation	Intensity	Orientation	Intensity	Orientation	Intensity
Radar entirely filtered	68.5°	0.14	150.5°	0.03	-135.4°	0.04
WRF precip. at 2830 m asl	22.6°	0.26	5.8°	0.24	-79.6°	0.19
WRF total ground precip.	30.6°	0.32	24.2°	0.24	-67.6°	0.21

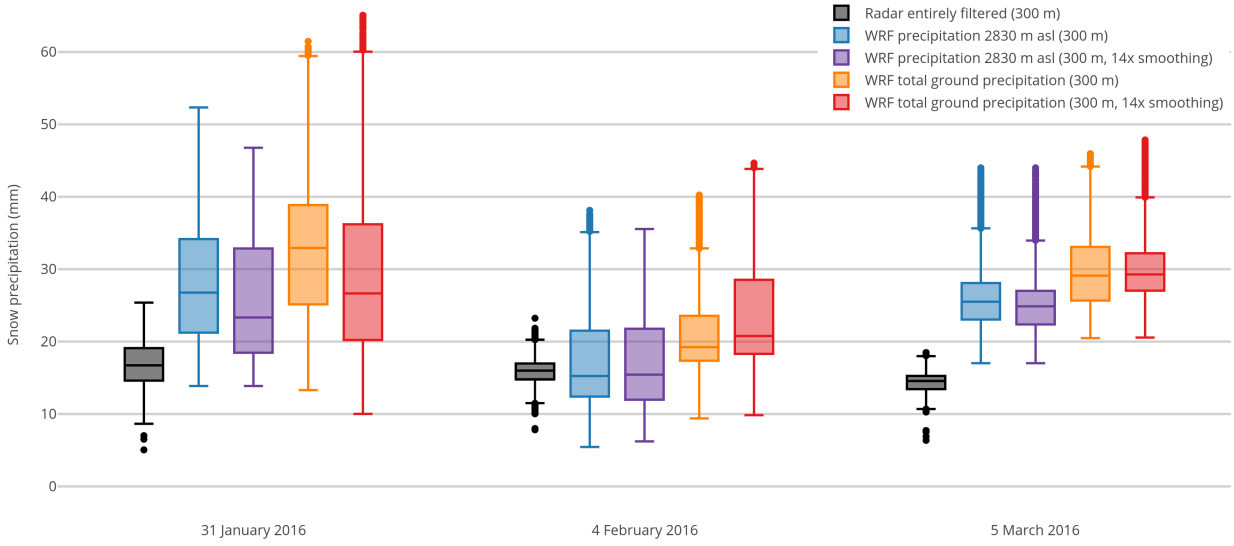

Figure S.1. Domain-wide 24 h precipitation statistics for the local domain (300 m resolution, Figure 1 in the main text) for the three precipitation events on 31 January 2016, 4 February 2016 and 5 March 2016. Gray colors show entirely-filtered radar precipitation. WRF precipitation at 2830 m above sea level (m asl) for simulations with weak terrain smoothing (Sect. 2.1 in the main text) and strong terrain smoothing are given in blue and violet, respectively. Orange (red) shows boxplots of WRF total ground precipitation for weak (strong) terrain smoothing. Radar precipitation and WRF precipitation at 2830 m asl are masked (as shown in Figure 4 in the main text).

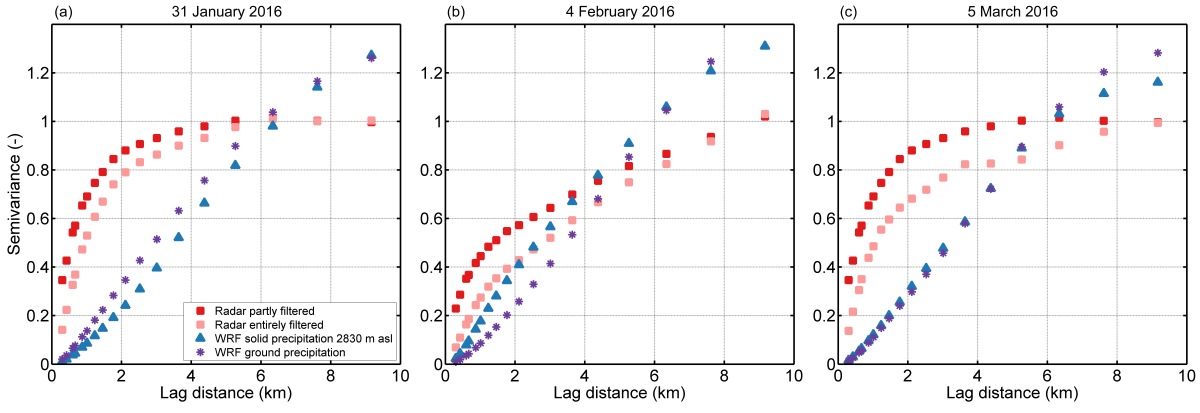

Figure S.2. Normalized variograms of detrended snow precipitation for the precipitation events on a) 31 January 2016, b) 4 February 2016 and c) 5 March 2016 for the local domain (Figure 1 in the main text). Variograms are given for partly-filtered (red) and entirely-filtered (orange) radar snow precipitation, WRF snow precipitation at 2830 m above sea level (m asl, blue) and WRF total ground precipitation (violet). WRF precipitation is from simulations with weak terrain smoothing (Sect. 2.1 in the main text). All precipitation fields are masked.

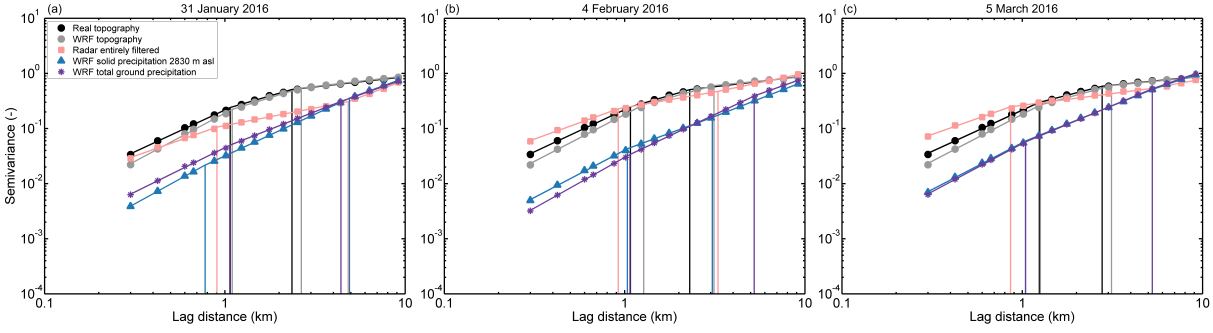

Figure S.3. Normalized variograms of the snow precipitation events on a) 31 January 2016, b) 4 February 2016 and c) 5 March 2016 for the local domain (Figure 1 in the main text). Variograms are given for entirely-filtered radar snow precipitation (orange), WRF snow precipitation at 2830 m above sea level (m asl, blue) and WRF total ground precipitation (violet). Additionally, variograms are given for real topography (based on dhm25 © 2018 swisstopo (5740 000 000), black) and WRF topography (gray). WRF topography and precipitation are from simulations with weak terrain smoothing (Sect. 2.1 in the main text). All precipitation fields are masked.